

8-1-2017

Numerical Study of Thermal Performance Improvement By Novel Structures in the Building Energy Storage Systems

Junling Xie

University of Wisconsin-Milwaukee

Follow this and additional works at: <https://dc.uwm.edu/etd>



Part of the [Mechanical Engineering Commons](#), and the [Oil, Gas, and Energy Commons](#)

Recommended Citation

Xie, Junling, "Numerical Study of Thermal Performance Improvement By Novel Structures in the Building Energy Storage Systems" (2017). *Theses and Dissertations*. 1726.

<https://dc.uwm.edu/etd/1726>

This Dissertation is brought to you for free and open access by UWM Digital Commons. It has been accepted for inclusion in Theses and Dissertations by an authorized administrator of UWM Digital Commons. For more information, please contact open-access@uwm.edu.

**NUMERICAL STUDY OF THERMAL PERFORMANCE
IMPROVEMENT BY NOVEL STRUCTURES IN THE BUILDING
ENERGY STORAGE SYSTEMS**

by
Junling Xie

A Dissertation Submitted in
Partial Fulfillment of the
Requirements for the Degree of

Doctor of Philosophy
in Engineering

at

The University of Wisconsin-Milwaukee

August 2017

ABSTRACT

NUMERICAL STUDY OF THERMAL PERFORMANCE IMPROVEMENT BY NOVEL STRUCTURES IN THE BUILDING ENERGY STORAGE SYSTEMS

by

Junling Xie

The University of Wisconsin-Milwaukee, 2017
Under the Supervision of Professor Chris Yingchun Yuan

In this work, numerical studies were conducted to investigate the effectiveness of two fin-like novel structures used for heat-transfer enhancement in two building energy storage systems, such as thermal energy storage and battery energy storage.

Firstly, thin layer ring structure was numerically investigated for thermal performance improvement in the thermal energy storage. From the results obtained in this study, the area ratio can be increased by 4% when using the thin layer ring during the same time period. The thin layer ring structure can shorten ice formation period and increase its efficiency. Further study was conducted for the factorial analysis of three parameters, including thickness, material and arrangement of thin layer ring. From the results, it shows that ice formation period can be shortened with the increase of conductivity and area of thin layer ring, while it is also dependent on thickness. Using Taguchi method, the statistic results show that material has the greatest impact on ice increased area. After that, arrangement has relatively less influence on ice increased area. However,

thickness has the trifling effect on ice increased area. The optimal combination of each factor (parameter) has been determined, and the optimal condition is A3B2C1. That is to say, for material = copper, thickness = 1mm, and arrangement = staggered, the best result of heat-transfer enhancement was obtained among all the cases studied. The reproducibility of these conditions has been verified by two analytical results.

Secondly, in battery energy storage, numerical simulations have been conducted to explore the air flow and heat transfer at different discharging rates in a horizontal rectangular channel with two different configurations of vortex generator(VG), such as rectangular rib and delta winglet. The simulation in air flow domain with characteristics of heat transfer and flow structure show that both types of vortex generators can enhance heat transfer before VGs, but only delta winglet VG can still enhance local heat transfer after it due to more vortices generated that can mix cold and hot air flow between the top and bottom thermal layers completely. The encouraging result shows that the maximum temperature of pouch cell can be decreased more by delta winglet than by rectangular rib. For the discharging rate at 5C, it can be decreased by 10% and the local Nusselt number can be increased by 38% compared to the baseline scenario without any VGs.

© Copyright by Junling Xie, 2017
All Rights Reserved

TABLE OF CONTENTS

ABSTRACT	ii
LIST OF FIGURES	ix
LIST OF TABLES	xi
LIST OF ABBREVIATIONS.....	xii
ACKNOWLEDGEMENTS	xiv
CHAPTER 1 INTRODUCTION	1
1.1 Introduction	1
1.2 Thermal energy storage.....	2
1.2.1 Sensible heat thermal energy storage	4
1.2.2 Latent heat thermal energy storage.....	5
1.2.3 Other PCM-based thermal energy storage.....	6
1.3 Battery energy storage.....	7
1.3.1 Electrochemical energy storage.....	7
1.3.2 Flow batteries	10
1.4 Research motivation and objectives	11
1.5 Summary and conclusion:	14
CHAPTER 2 LITERATURE REVIEW	18
2.1 Literature review	18

2.2 Principle of enhancement using extended surface	18
2.3 Ice Thermal energy storage	20
2.3.1 Recent studies of ITS thermal performance improvement	22
2.3.2 Fin-like thin layer ring to improve ITS thermal performance	24
2.4 Battery energy storage.....	26
2.4.1 Current studies of BESS thermal performance improvement	28
2.4.2 Fin-like vortex structure to improve BESS thermal performance	31
2.5 Vortex generator technique	32
2.5.1 Delta winglet.....	32
2.5.2 Delta wing.....	37
2.5.3 Rectangular winglet.....	38
2.5.4 Impact of different parameters	39
2.5.5 Summary of vortex generator	42
2.6 Taguchi method.....	44
CHAPTER 3 NUMIERICAL STUDY OF THIN LAYER RING IN THERMAL ENERGY STORAGE SYSTEM	46
3.1 Introduction	46
3.2 Model description.....	46
3.2.1 Physical model.....	46
3.2.2 Governing equations.....	48

3.2.3 Boundary conditions.....	50
3.2.4 Solution method and grid independence validation	52
3.3 Results and discussion of thin layer ring study in ITS system.....	54
3.3.1 Ice formation in one cylinder rectangular space.....	54
3.3.2 Ice formation in four cylinder rectangular space.....	56
3.4 Factorial effect analysis on thermal performance	58
3.4.1 Heat transfer enhancement using thin layer ring	58
3.4.2 Effect of material	59
3.4.3 Effect of thickness	62
3.4.4 Effect of arrangement	66
3.5 Factorial effect analysis of thin layer ring by Taguchi method	68
3.5.1 Selection of characteristics	69
3.5.2 Factor and levels.....	69
3.5.3 Orthogonal array.....	70
3.5.4 SN analysis	70
3.5.5 Taguchi Analysis	72
3.5.6 Determination of the optimal condition.....	74
3.5.8 Reproducibility by confirmation test.....	75
CHAPTER 4 NUMERICAL STUDY OF VORTEX STRUCTURE IN BETTERY ENERGY STORAGE SYSTEM	79

4.1 Introduction	79
4.2 Numerical model description	79
4.2.1. Physical model.....	79
4.2.2 Flow domain:	83
4.3 Numerical method and parameter definitions	85
4.4 Solution method and model validation.....	87
4.5 Results and discussion.....	89
4.5.1 Heat transfer	89
4.5.2 Flow structure	98
4.6 Conclusion.....	102
CHAPTER 5 CONCLUSIONS AND FUTURE STUDIES.....	103
5.1 Main results by using fin-like structures in two building energy storages.....	103
5.1.1 Main results of thin layer ring application.....	103
5.1.2 Main results of vortex generator application	105
5.2 Recommendation for future study.....	106
REFERENCES	108
CURRICULUM VITAE.....	117

LIST OF FIGURES

Figure 1. 1 Energy Consumptions in the U.S.	1
Figure 2. 1 Temperature distribution in a typical counter-flow heat transfer area	19
Figure 2. 2 Energy consumption in commercial buildings by end use	21
Figure 2. 3 Mechanism of enhanced heat transfer	25
Figure 2. 4 Different levels of battery thermal management	28
Figure 2. 5 A schematic showing the longitudinal vortices generated by a delta wing.....	32
Figure 3. 1 Geometry of the ITS tank (Left) and the analyzed rectangular space	47
Figure 3. 2 One cylinder and four cylinders rectangular space	48
Figure 3. 3 Mesh distribution.....	52
Figure 3. 4 Validation of numerical model.....	53
Figure 3. 5 Ratio of A_i/A_c with different grid number at 900s	53
Figure 3. 6 Temperature distribution	54
Figure 3. 7 Liquid fraction distribution.....	55
Figure 3. 8 Cavity during ice formation.....	56
Figure 3. 9 3D geometry of thin layer ring	56
Figure 3. 10 Comparison of liquid fraction at 7200s	57
Figure 3. 11 Liquid fraction (left) Temperature (right)	60
Figure 3. 12 Temperature variation in the middle vs. time.....	61
Figure 3. 13 Liquid fraction (left) Temperature (right)	63
Figure 3. 14 Temperature variation in the middle vs. time.....	64

Figure 3. 15 Liquid fraction (left) Temperature (right): A (without ring), B (staggered), C (1 parallel), D (2 parallel).....	66
Figure 3. 16 Temperature variation in the middle vs. time.....	67
Figure 3. 18 SN ratio on each factor	74
Figure 3. 17 Contribution ratio on each factor.....	74
Figure 3. 19 Time-wise temperature during ice formation	77
Figure 3. 20 Liquid fraction and temperature distribution of condition 1 and condition 2	77
Figure 4. 1 Geometry of Pouch Cell.....	80
Figure 4. 2 Validation of grid number	87
Figure 4. 3 Potential curve between experimental and numerical studies	88
Figure 4. 4 Temperature curve between experimental and numerical studies.....	88
Figure 4. 5 Local heat flux of rectangular rib and delta winglet at 0.5c, 1c, 2c, 3c, 5c.....	90
Figure 4. 6 Illustration of flow domain.....	91
Figure 4. 7 Buck mean temperature of three scenarios at 5 different C rates.....	93
Figure 4. 8 Nusselt number of three scenarios at 5 different C rates.....	96
Figure 4. 9(a) Flow structure of rectangular ribs (b) Flow structure of delta winglet	98
Figure 4. 10 Half-cross sections of velocity vectors.....	100
Figure 4. 11 Time-wise maximum cell temperature and potential of pouch cell	101

LIST OF TABLES

Table 2. 1 Comparison of global effects of four VGs.....	40
Table 3. 1 Dimensions of analyzed space.....	48
Table 3. 2 Thermo-physical properties of water in the study	51
Table 3. 3 Baseline of thin layer ring.....	58
Table 3. 4 Investigated parameters	59
Table 3. 5 Levels of each factor.....	70
Table 3. 6 The orthogonal array of L9.....	71
Table 3. 7 SN ratio on each case.....	71
Table 3. 8 Factorial effect and contribution ratio	73
Table 3. 9 Optimal conditions from factorial effect analysis.....	75
Table 4. 1 Property of the constant values	82
Table 4. 2 Parameters used for the thermal modelling	82

LIST OF ABBREVIATIONS

A_i	ice area
A_c	cylinder area
c	specific heat, J/kg K
C_s	specific heats of solid phase
C_l	specific heats of liquid phase
d	diameter of the cylinder
g	acceleration of gravity, m/s ²
h	sensible enthalpy, J/kg
$h_{reference}$	reference enthalpy
k	thermal conductivity, W/mK
K	Permeability, m ²
K_0	empirical constant in Kozeny-Carman equation
L	latent heat, J/kg
P	pressure, Pa
t	time
T_f	fusion temperature, 273.15K
u, v	x, y direction velocity vector components
U, V	x, y direction dimensionless velocity-vector component
x, y	Coordinate axes
i	Linear current density
J	Current density
r	Resistance
V	Potential (V) of battery cell
Y, U	Fitting parameters in polarization expression
u_m	Mean air velocity
Nu	Nusselt number

h_x	Local heat transfer coefficient
q_x	Average heat flux

Greek symbols

β	liquid volume fraction
μ	dynamic viscosity, N s/m ²
ρ_m	max density of water, 999.972 kg/m ³
Ω	Domain

Subscripts

i	initial condition
L	liquid phase
s	solid phase
ref	reference value
w	cylinder surface
p	Positive electrode
n	Negative electrode

ACKNOWLEDGEMENTS

In the past five years of my PhD study, I received tremendous support and encouragement from a great number of great people. Firstly, it is my great honor and pleasure to express my deepest gratitude to my dear Professor Chris Yuan for his inspiration and professional guidance that helped me achieve a thoughtful and rewarding journey. Without his diligent efforts, numerous support, helpful advice and endless encouragement, this work would not have been possibly completed. Secondly, I would also extend my sincere gratitude to all dissertation committee of Dr. Benjamin Church, Dr. John Reisel, Dr. Wilkistar Otieno and Dr. Ilya Avdeev for their everlasting support and guidance on my research skills that I developed significantly.

Without financial support, this study could not have been finished. I would like to thank U.S. Department of Energy, the Engineering Department (University of Wisconsin Milwaukee) for their generous sponsorship. In addition, the great support that I received from all my lab friends (Laboratory for Sustainable and Nano-Manufacturing, Industrial Assessment Center) is also acknowledged.

Finally, I would like to thank my family and my wife, Jingyi for their loves and understandings, who have always been there cheering me up, standing by me at good and bad moments.

CHAPTER 1 INTRODUCTION

1.1 Introduction

In the United States, the building sector is responsible for about 40% of the total energy consumption and accounts for nearly 40% of greenhouse gas emissions as shown in Figure 1.1 (McQuade 2009). The improvements of building energy efficiency, by relatively optimistic goals of 50%-70% above ASHRAE Standard 90.1-2004, suggest reductions in the total carbon emissions attributable to buildings. However, population and economic growth will continuously increase total area of buildings, which makes the total reduction of emissions an even harder goal to reach.

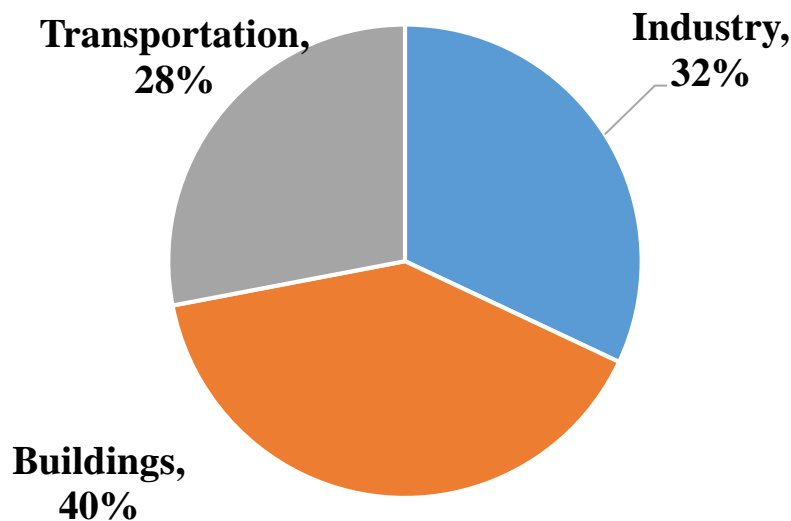


Figure 1. 1 Energy consumptions in the U.S.

Per DOE, to achieve long-term greenhouse gas reduction targets by 2050 is inextricably related our ability to decarbonize the energy supply to the U.S. building sector. The building sector is

perfectly positioned, not only to contribute by drastically improving energy efficiency on the demand side, but also to contribute to the supply side by providing grid services with potentially no carbon emissions penalties. Therefore, building energy management technologies play the more and more important roles in greenhouse gas reduction and sustainable buildings.

Nowadays, various energy storage technologies have been applied to meet the energy, environmental and economic challenges and addressed growing building energy demand, because energy storage can harvest excess energy during periods of low demand and return the stored energy when it is needed during peak usage periods. Furthermore, the storage devices can also play the role of reserve power plants so as to provide extra energy in case of power system contingencies or a rapid change in demand (Reihani, Sepasi et al. 2016). Among all energy storage technologies, the most popular building-scale energy storage technologies are based on thermal or electrochemical storage mechanisms, such as batteries and thermal energy storage that have become increasingly import recently for peak-load shifting in the building energy systems (Kintner-Meyer 2010). The improvement of these two storage systems can benefit energy management in the building sector significantly as well (Ikeda and Ooka 2015).

1.2 Thermal energy storage

Nowadays, using energy storage can achieve operational flexibility for a building or an electric grid. Thermal energy storage (TES) equipment can reduce the demand charge and electricity cost during peak periods. The simply operational strategy of storage is to be charged during low-cost off-peak periods and then discharged during peak periods. Therefore, thermal energy storage is

used to reduce the electricity bill by shifting air-conditioning loads to low-cost off peak periods. In some cases, thermal energy storage can also be used to provide additional cooling capacity when direct cooling equipment is insufficient to meet cooling demand during peak periods. That thermal energy storage has become a cooling load management tool to generate value for the electricity service provider in exchange for a financial reward for the building owner. Key benefits are higher utilization of the energy infrastructure, higher reliability, and more effective load and outage management. The deferment of investment on utility infrastructure may delay a rate increase or slow down the rate at which electricity rates may increase in the future.

Thermal storage categories include both sensible thermal and latent thermal options. Sensible thermal options include storage in the elements of building construction (structural and non-structural) and hot or chilled water storage. Latent thermal options are expected to be dominated by ice storage, but could include other phase-change materials (PCM) systems, including PCMs integrated into the building envelope components.

Thermal energy storage has the advantage of direct use in achieving building space conditioning, since it is on-site option to directly supply cooling energy for the whole building application. Typically, the application of thermal energy storage in a building can provide significant smoothing capabilities, such as reducing cooling energy for the building during on peak periods and reducing electricity cost and electricity demand requirement.

Thermal energy storage (TES) is a proven technology that is dependent upon space-availability. If space is available, chilled water storage as sensible thermal option is preferred because of high chiller efficiency. Otherwise, ice thermal storage as latent thermal storage is preferred in space constrained applications. A critical parameter for the practical application is storage density which is usually expressed in energy units per unit volume. If the operational temperature range during charging and discharging depends on the melting and solidification temperature of the storage medium, the TES technology is latent thermal storage. For latent thermal storage, the storage medium is a phase change material (PCM). If no phase change occurs, the storage is sensible thermal storage.

1.2.1 Sensible heat thermal energy storage

Currently available sensible TES includes building thermal mass storage, ground (seasonal) thermal storage and chilled-water storage in a typical building. Energy as heat is usually stored by the temperature change of a storage medium, such as water, air, oil, rock beds, bricks, concrete or sand. The energy stored is proportional to the temperature rise as expressed by the following equation.

$$E = m \times C \times \Delta T \quad (1.1)$$

Where,

E = Stored energy

C = Specific heat capacity of the storage medium

T = Temperature change

Therefore, the total stored energy depends on the heat capacity of storage medium, the temperature change and thermal mass. This type of thermal storage is the most common method of cold storage. By pre-cooling the building thermal mass, building mass thermal storage can successfully shift cooling loads to off-peak periods at night without compromising thermal comfort. It works as a building jacket out of conditioning spaces.

For a ground (seasonal) storage, since the near surface ground almost remains a constant temperature throughout the year, the ground surrounding and/or underneath the building for seasonal thermal energy storage has become an approach for storage. This approach is to store energy in the ground during the summer and is used during the winter. Conversely, the ground is cooled to store cooling energy in winter and release to the building in summer.

Another matured technology in sensible TES is chilled water storage. However, space constraint is usually an issue in the most commercial buildings for chilled water storage, which can favor ice-storage technologies due to the higher energy density. Owing to its simplicity and low first cost, chilled-water storage is still used in some commercial buildings.

1.2.2 Latent heat thermal energy storage

Latent heat thermal energy storage is to utilize a phase change material (PCM) to store energy during melting and solidifying processes. This technology can store and release large amounts of energy.

Typically, ice is the most commonly used PCM for latent heat TES. With a specific heat of fusion of water of about 333 kJ/kg, compared to the specific heat of water of about 4 kJ/(kg*K), the volume of a chilled water tank requires about 8-10 times larger than that of an ice storage.

Recently, ice thermal storage system is commercially in a wide variety of manufacturers that differ in the heat exchanger configurations, method of ice containment, and other engineering details. Generally, the categories of ice thermal storage technology include internal-melt ice on coil, external-melt ice on coil, encapsulated, ice harvester, and ice slurry technologies. The ice solidification process basically form ice on cooling coil.

1.2.3 Other PCM-based thermal energy storage

There are other PCMs adapted in the thermal energy storage systems with non-ice PCMs. Salt hydrates as phase change materials usually freeze above the melting point of ice, so the operational cost of these non-ice PCM thermal storage systems are not very cost-effective compared to ice-based PCM thermal energy storage. Therefore, it is barely seen that non-ice PCMs thermal energy storage are commercialized widely. Even though other PCMs have been proposed and tested for enhancement of the thermal mass of envelope components for many years, those technologies have not been massively applied in the building because of high initial cost, gradual deterioration of the phase-change properties, material leakage, and corrosion. However, PCM-enhanced wall board is still commercially available.

1.3 Battery energy storage

Battery energy storage is the other most popular storage technology commercially for building applications. The most common applications of battery energy storage are uninterruptable power supplies (UPS) in data centers, telecommunications or sensitive processes.

Battery energy storage as electrical options include both conventional and flow batteries. There are several technology-category levels of current battery energy storage.

1.3.1 Electrochemical energy storage

Electrochemical energy storage as one option can broadly be classified into conventional and flow batteries. Conventional batteries include lithium-ion, nickel-metal-hydride, nickel-cadmium, lead-acid, and sodium-sulfur batteries. Flow batteries include zinc-bromine and vanadium-oxide batteries. Flow batteries are normally considered for relatively larger than 1 kWh stationary applications.

1.3.1.1 Lithium ion battery (Li-ion)

The main advantages of Li-ion batteries, compared to other advanced batteries, are (Divya and Østergaard 2009):

1. High energy density (225-375 Wh/L, 90-150 Wh/kg)
2. Room for further improvement with high voltage cathodes and electrolyte
 - a. High efficiency (80-85% DC to DC)
 - b. Diverse chemistry to target different operation regimes (high power vs. high energy)

c. Long cycle life (3000 cycles at 80% DOD).

While Li-ion batteries have almost dominated battery market, there are some challenges for large-scale Li-ion batteries. The main concerns are the high cost, complex battery management circuitry, and safety issues related to thermal management.

1.3.1.2 Nickel metal hydride battery (NiMH)

The specific energy of NiMH is lower compared to the lithium-ion cell. The tolerance to high temperature excursions is also relatively poor. Even though it has a relatively high self-discharge rate, the capacity loss usually reaches up to 50% of its original capacity after 6 months of storage. Hence nickel metal hydride battery is obviously not a good candidate for building battery energy storage.

1.3.1.3 Nickel cadmium battery (Ni-Cd)

Ni-Cd batteries have a high-power density, and are used in most power tools and equipment due to its rugged characteristic. Cylindrical Ni-Cd batteries are mostly used in consumer electronics and power tools, while prismatic Ni-Cd batteries are used in large stationary applications. Furthermore, DC to DC efficiency for Ni-Cd batteries ranges from 60 to 70%. Flooded batteries last longer while rated to last 10 to 15 years. Sintered plate Ni-Cd batteries can achieve 3,500 cycles at 80% DOD. Their self-discharge rate of Ni-Cd is 5% per month, which is approximately five times higher than that of lead acid batteries. In such large battery system with

Ni-Cd, it usually includes active thermal management along with hydrogen sensing and ventilation.

1.3.1.4 Lead acid battery

One of the oldest and most developed battery technologies is lead-acid. Due to its short cycle life at high depth of discharge (1000 cycles vs. 3000 cycles for Li-Ion) and low specific energy and energy density, its application for energy management has been very limited. Typically, lead acid batteries are used for vehicle starting, lighting and ignition (SLI) with high power and shallow depth of discharge. Moreover, it is also used in stationary applications for traction purposes with deep depth of discharge. DC to DC efficiencies range from 75% to 85%. The cycle life at 100% DOD varies from 100 for SLI batteries to 1000 for deep cycle batteries.

1.3.1.5 Sodium sulfur (Na-S) battery

Na-S battery cells have a DC to DC efficiency of 80%. With thermal management, the Na-S battery can provide above its rated power output (Ibrahim, Ilinca et al. 2008). For instance, the Na-S battery can deliver 500% of rated power over five minutes, 400% of rated power over 15 minutes, and 260% over one hour, with power rated at the seven-hour rate. Hence the maximum DOD at the 1-hour rate is only 37%. To prevent cell temperature from over being heated, thermal management can overcome this limitation. The cycle life as a function of depth of discharge varies from 4000 cycles at 90% DOD to 43,000 cycles at 10% DOD. The only supplier for this battery technology is NGK Insulators, Ltd. The total installed capacity in the year 2007 was 270 MW, which increased to 630 MW by the end of 2010. Nearly 45% of the installed systems are used

for electricity load leveling, and 40% for emergency power/uninterrupted power system (UPS), with about 13% used for renewable energy storage.

1.3.2 Flow batteries

1.3.2.1 Zinc bromine flow battery

The Zn-Br battery can be classified into a power module that combines cell stack and electrolyte circulation. The energy system module of Zn-Br battery consists of electrolyte storage tanks (Ponce de León, Frías-Ferrer et al. 2006). Since the power and energy modules are independent, higher power systems can be achieved by increasing the number of modules.

The DC to DC efficiency for Zn-Br Flow Battery is 70% to 80%. Zn-Br batteries self-discharge rates at nearly 1% per hour due to bromine crossover. If electrolyte flow stops, mitigation of self-discharge can stop as well. If thermal management is poor during self-discharge, temperature of batteries increases significantly.

1.3.2.2 Vanadium oxide flow battery

The efficiency of this battery can be as high as 85%. The power and energy ratings are the same as other flow batteries that are independent of each other. The use of Vanadium Oxide Flow Batteries has increased continuously due to independence of power and energy subsystems (Gattrell, Park et al. 2004). The disadvantage of such batteries compared to other flow batteries are low energy density (20-30 WH/L; 15-23 WH/kg), low power density, high self-discharge

rate, high bipolar plate cost, high membrane and reactant cost. However, VRB systems have a very fast response time.

1.4 Research motivation and objectives

The research is to study the thermal performance improvement by using two novel structures in ITS and BESS so as to evaluate the benefits and penalties of two new techniques and to understand the improved heat transfer associated with flow field characteristics and their mechanisms underneath.

Because of the large parameter space, carrying out experimental study is expensive and time consuming for the new innovated devices, and a numerical method would be more viable for such investigation. With the rapid growth of computing technology, it is more possible and practical to obtain numerical predictions of the impact of two novel structures (thin layer ring and vortex generator) in ice thermal storage system and battery energy storage system. With the numerical method, the proposed research will be focused on three main objectives. The first one is to investigate the performance of thin layer ring with different parameters and configurations, so as to develop a better understanding of ice formation process and attendant heat-transfer behavior in a typical ITS system embedded with thin layer ring and how it could be designed to improve energy efficiency of the ITS system. The second one is to examine the performance of VG with different parameters and configurations in BESS application, so as to get a better understanding of the flow structure and attendant heat-transfer behavior and provide a guideline of the implementation of VG in BESS. Finally, the third objective is to conduct a study of the parametric impact on the

performance of two novel structures by Taguchi Method and find the optimal combination of parameters for the design guideline of two novel structures.

Therefore, the numerical method is adopted to evaluate both structures' impact on thermal performance enhancement in ITS and BESS. The first investigation is focused on the performance of thin layer ring with different parameters and configurations in ITS, so as to develop a better understanding of ice formation process and attendant heat-transfer behaviour in a typical ITS system embedded with thin layer ring and how it could be designed to improve energy efficiency of the ITS system.

- Numerical Study in ITS:
 1. Create a numerical model of ice formation in the ice thermal storage domain.
 2. Numerically investigate ice formation process and associated heat transfer performance before and after thin layer ring adopted.
 3. Advance the understanding of how ice formation process near thin layer ring would be improved.
 4. Analyze temperature variation along with ice formation period.
 5. Examine a wide range of influencing parameters, such as material, thickness, arrangement of thin layer ring.

The second objective is to conduct a study of the parametric impact on the performance of thin layer ring structure and evaluate factorial effect of different parameters for the design guideline of thin layer ring. The detailed research goals are:

- Parametric Study of thin layer ring structure in ITS

1. Select the main categories of the performance characteristics.
2. Determine the number of levels of each factor in order to perform the comparison study of each parameter.
3. Choose a suitable orthogonal array for experiments.
4. Conduct S/N analysis based on the selected characteristics, such as the larger the better, the nominal the better or the smaller the better.
5. Conduct statistical analysis using the Taguchi method to predict the contribution ratio of each parameter.
6. Determine the optimal combination of each parameter.

The Third objective is to examine the performance of vortex generator with different parameters and configurations in BESS application, so as to get a better understanding of the flow structure and attendant heat-transfer behaviour and provide a guideline of the implementation of VG in BESS.

A numerical model of a Li-ion pouch cell coupled with air flow as cooling on its surface will be created. The following research is based on this model to investigate air flow structure and heat transfer performance in a rectangular, horizontal cooling channel with VGs embedded. Detailed data related to thermal and fluid will be exported from Fluent to quantify heat transfer enhancement associated with pressure drop penalties. Therefore, this study is to advance the understanding of how longitudinal vortices generated by VGs interact with each other, and how the interaction affects thermal-hydraulic behavior with VG used on the surface of a Li-ion pouch cell. With a

better understanding of the mechanisms of heat transfer enhancement using VG, a wide range of influencing parameters will be examined. Heat transfer enhancement and associated flow structure will be quantified. The goal is to understand how these parameters will influence overall thermal performance, in order to develop a design guideline for further study or application of vortex generation techniques in BESS.

- Numerical Study in BESS

1. Create a numerical model of Li-ion pouch cell unit coupled with air flow as cooling on its surface.
2. Numerically investigate the discharging phase of Li-ion pouch cell unit to predict a suitable location of VG.
3. Analyze air flow structure and heat transfer performance on a Li-ion pouch cell surface with VG embedded.
4. Advance the understanding of how longitudinal vortices behind different VGs interact with each other and how the interaction affects the thermal-hydraulic behavior.
5. Quantify associated heat transfer enhancement and present flow structure.

1.5 Summary and conclusion:

As sophisticated technologies to store energy, thermal energy storage and battery energy storage were firstly created to reduce the total demand of building electricity and avoid expensive distribution system upgrades. Thus, the building owners can reduce the demand charge component of the electricity bill. Secondly, electricity load shifting could shift energy use from

on-peak periods to off-peak periods, which reduce electricity charged to the difference of electricity rate between on-peak periods and off-peak periods. Since the building can almost utilize all electricity demand, there is an incentive to maximize cost saving owning to high power factor during on-peak periods.

As of now, both energy storage technology has been gradually adapted in renewable technologies with increased penetration of wind and solar energy generation. Since grid operators need to produce more balanced energy production and reserve generated energy. Energy storage has been expected to play into this growing market place. The most direct way to accommodate balancing services includes battery energy storage that can release and absorb electric energy to and from the grid. This may also be accomplished indirectly through a thermal energy storage system. In this case, the end-use load of cooling equipment would modulate its output in accordance with cooling load requirements and grid needs.

The integration of energy storage and renewable energy technologies are taking place in the U.S. The transition of today's grid to a modern energy infrastructure will both enable and require much more active participation of load customers in the energy and ancillary services markets. Ubiquitous communications technologies and advanced controls will transform resources in the demand sectors from passive to active elements on the grid. "Smart" commercial buildings will not be the sole active demand side participants on the emerging smart grid, as sophisticated home energy management systems will enable the residential building sector and smart charging

strategies will link in the electric vehicle fleet. Likewise, bulk energy storage technologies, smaller community energy storage systems, and on-site battery storage are also likely to compete in these new markets.

TES is proven technology. Choice of the TES dependence on space-availability of storage tank. If space is available, cold-water storage is preferred because of high chiller efficiency. If ice-storage is desirable because of space constraints, then chiller efficiency is likely to be reduced because of larger delta T or low chilled water temperature. Phase change materials integrated into building materials is novel technology- not currently used. Advantage would be that its storage would not require dedicated location and footprint for storage tank, such as PCM building jacket.

Currently, there are many proven battery chemistries in commercially available systems applicable for buildings applications. Most batteries have been used for uninterruptable power supply (UPS) in data centers or for other high-sensitive processes in buildings. UPS is rarely used only when line power fails. The integration of batteries for load time-shifting strategies are not common and would need to be custom-designed at high cost.

Battery storage systems on-site in commercial buildings for applications other than dedicated UPS applications are not common. Although there are not many technical barriers that would limit the use of battery storage for time-shifting of buildings loads and/or supporting integration of intermittent renewable technologies, the cost is still relatively very high. The only two barriers are related to battery capacity and thermal management.

The improvement of these two storage systems can benefit energy management in the building sector significantly. This research focused on thermal performance improvement by using two novel structures in ITS and BESS will evaluate the benefits and penalties of two new techniques and also give a better design guideline to improved heat transfer associated with flow field characteristics and their mechanisms in both building energy storage systems.

CHAPTER 2 LITERATURE REVIEW

2.1 Literature review

The literature review has been conducted based on thermal energy storage, battery energy storage technologies. Since this study is to enhance heat transfer in both common building energy storage systems using extended surface, the basic principle behind the enhancement mechanism is presented first. Secondly, literature review is to examine the current technical challenges and address relevant approaches to improve their performance and overcome those technical obstacles. For ice-thermal storage system, the focus is on the improvement of ice formation process and attendant heat transfer enhancement in the storage system. For the battery energy storage system, thermal management system is important, the emphasis of review is on the thermal performance improvement and adopted approaches in its research field. Due to the large parameter space, Taguchi method is also reviewed for the statistical analysis of these parameters.

2.2 Principle of enhancement using extended surface

The heat-transfer rate can be enhanced by changing the surface geometry in typical heat transfer area. The principle of enhancement is explained as follows. The heat exchange rate can be calculated as

$$q = UA\Delta T_m \quad (2.1)$$

where q is the rate of heat transfer, U is the overall heat transfer coefficient based on area A , which can be the hot-side area (A_i) or the cold-side area (A_o). ΔT_m is the logarithmic mean temperature difference (LMTD) defined as:

$$\Delta T_m = \frac{(\Delta T_2 - \Delta T_1)}{\ln\left(\frac{\Delta T_2}{\Delta T_1}\right)} \quad (2.2)$$

where $\Delta T_1 = (T_{h1} - T_{c2})$ and $\Delta T_2 = (T_{h2} - T_{c1})$ are the temperature differences between the hot and cold fluids in the heat transfer area or surface, as shown in Fig.2.1.

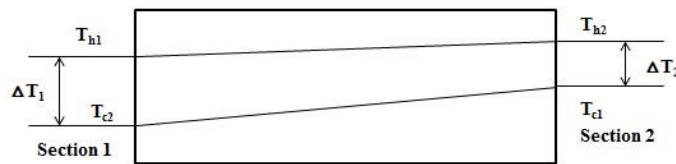


Figure 2. 1 Temperature distribution in a typical counter-flow heat transfer area

The overall thermal resistance is defined as follow:

$$\frac{1}{UA} = \frac{1}{h_i A_i} + \frac{1}{h_o A_o} + \frac{t}{kA} \quad (2.3)$$

where A_i and A_o are the hot-side and cold-side heat transfer areas respectively; h_i and h_o are the corresponding convective heat transfer coefficients; t is the thickness of heat transfer material; k is the thermal conductivity of the material and A is the average of the both cold and hot heat transfer areas of the heat exchange medium. When the surfaces are enhanced, the thermal resistance of the enhanced system is presented as follow:

$$\frac{1}{UA} = \frac{1}{\eta_1 h_i A_i} + \frac{1}{\eta_2 h_o A_o} + \frac{t}{kA} \quad (2.4)$$

where η is the efficiency of the extended surfaces. η_1 and η_2 are smaller than 1.0 so that they can reduce the overall thermal resistance. If the heat-transfer areas (A_i and A_o) or the heat-transfer coefficients (h_i and h_o) are enhanced, thus heat-transfer rate increases. The modification of surface geometry can effectively help enhance the heat transfer. Webb (Webb 1994) described a large number of methods for the air-side heat transfer enhancement. These methods include treated surface, rough surface, extended surface, displaced enhancement devices, etc.

2.3 Ice Thermal energy storage

As shown in Figure 2.2, among all the energy used in the building sector, air conditioning and other cooling operations take a share of 16~50% of the electricity consumption (Saidur, Masjuki et al. 2007). Recently, ice thermal storage (ITS) systems have been widely used to store the electrical energy in ice formation during off-peak hours and release the stored energy during peak hours for cooling purposes, so to reduce peak demand charges. With the ice thermal energy storage, the offset in electricity demand is accompanied by an improved system performance (MacCracken 2003) and reduced total cost (1996). Therefore, ITS is a good on-site storage option to store the electrical energy in ice formation during off-peak hours and release the stored energy during peak hours for cooling purposes, so to reduce peak demand charges. This is a cycling process for energy transfer and conservation. Although energy conservation is popularly studied, peak demand conservation was not properly addressed until recently (Shears 1991, Redindel 1996, Hasnain 1998). Peak demand is important because utility companies always require supplying sufficient

energy to accommodate the expected increases in peak demand. Because of varying structures of electricity rates and the offered incentives, ITS system has been regarded as the most advanced and cost effective peak demand management method for space cooling (H. Akbari 1989, Sumpter 1992, Brower 1994, Rismanchi, Saidur et al. 2012) in different building applications that are mainly occupied during the operating hours, such as office buildings(Chaichana, Charters et al. 2001), hospitals(T. Collins 2000), schools(Haughey 2003, S. Morgan 2010), and churches and mosques(Habeebullah 2007).

Percent of Total Consumption in Commercial Buildings by End Use

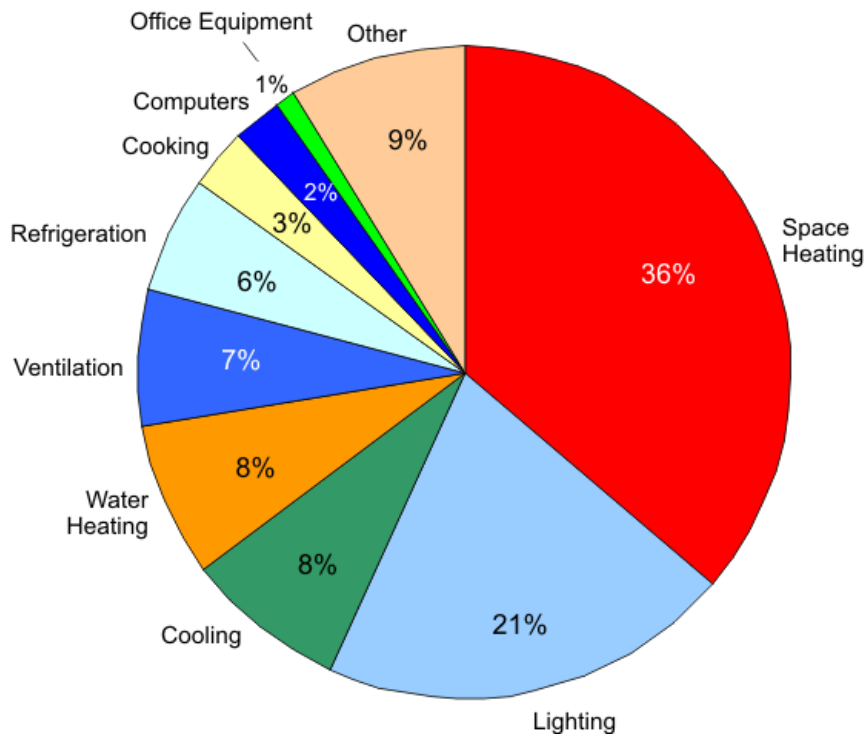


Figure 2. 2 Energy consumption in commercial buildings by end use

ITS systems effectively shift peak electricity demand to off peak as a part of the effective strategies for energy management in buildings. Such a strategy can reduce on-peak loads while it will increase the load during off peak periods for the utility companies. This shifting of load greatly improves the utilization of basic power generators by reducing the reliance on peaking units which typically have higher operating costs. ITS systems also provide great benefits for the electricity customers by utilizing off peak electricity which usually has a lower electricity rate thus reducing the monthly demand charge. Conventional cooling systems in buildings use a standard chiller to produce ice at night during off-peak periods. The refrigeration system could be in use during the off peak night time hours when the cooling load and electricity rate are low. During the day time, cooling can be supplied by circulating the cooling refrigeration from an ITS system rather than operating the chiller. Advantages could be reflected on the electric consumer, with lower energy cost and better space cooling. The utility company would also benefit, with higher electric load factor and lower capital investment in new generating equipment.

2.3.1 Recent studies of ITS thermal performance improvement

Nowadays, water or ice are the most attractive storage materials for HVAC field and have been widely used as phase change material (PCM) (2007), since these materials are inexpensive, abundant and safe (Yamaha, Nakahara et al. 2008). However, in the current ITS systems, the solidification of ice is not well developed which not only affects the cooling performance of the system but also wastes energy.

In order to improve heat transfer performance in ice thermal storage system, many methods have been studied and explored in the past. Some methods have been carried out for the heat transfer enhancement with fin configurations. The application of fin with different configurations has been proposed by various researchers as an efficient means to improve the charge and discharge capacity of the thermal storage system. Sparrow et al. (E.M. Sparrow 1984) experimentally performed studies for the outward solidification on a longitudinal finned vertical tube for conduction-controlled or natural convection-controlled heat transfer. They found that the ice formation could be enhanced by placing fin on the vertical tube. A theoretical model was presented by Lacroix (Lacroix 1993) for predicting the transient behavior of a shell-and-tube storage test unit with annular fins externally mounted on the inner tube with the PCM on the shell-side and the HTF flowing inside the tube. Padmanabhan and Krishna Murthy (P.V. and M.V. 1986) have also studied the phase change process occurring in a cylindrical annulus where annular fins are attached to the outer surface of the inner isothermal tube, while the outer tube is made adiabatic. Parametric study has been analyzed and they have suggested working formulae to obtain the volume fraction solidified at any time for both the cases.

Research was also conducted on the heat transfer enhancement by modifying phase change material. Siegel (Siegel 1977) has studied the improvement and solidification rate in molten salt dispersed with high conductivity particles. His study shows that even though there is improvement in the heat transfer rate, there is a compensating effect due to the reduction in volume fraction occupied by the phase change material. Some results obtained by Hoogendoorn and Bart (C.J. Hoogendoorn 1992) show that the low value of the thermal conductivity of the PCMs could be

greatly improved by embedding a metal matrix structure in them. Khan and Rohatgi (M.A. Khan 1994) have studied the heat transfer characteristics during solidification in the presence of cylindrical reinforcements, including graphite, alumina, iron, and copper in an aluminium-silicon alloy-base and lead-base composites. They reported that the rate of movement of interface is strongly dependent on the thermal conductivity ratio of reinforcement of the melt, which means the reinforcement added with higher thermal conductivity can increase the rate of solidification.

2.3.2 Fin-like thin layer ring to improve ITS thermal performance

Current technical performance of ice thermal storage (ITS) has a large impact on continuously improving the energy efficiency and reducing the environmental impact of buildings. In the current ITS systems, the ice formation is not well developed which not only affects the cooling performance of the system but also wastes energy. In particular, there are some blind areas between the refrigerant cylinders with incomplete ice formation due to inefficient heat transfer which lowers the thermal storage capacity of the system (Xie and Yuan 2014). The rate of ice formation depends on three major heat transfer processes as shown on the top of Figure 2.3; convection from the heat transfer fluid (refrigerant) to the refrigerant cylinder, conduction within the cylinder, and heat transfer from cylinder to the phase change material (PCM) such as water through conduction and/or convection. In the solidification process, the solid layer generated by PCM on the cylinder surface reduces the heat transfer rate (Chiu, Martin et al. 2009).

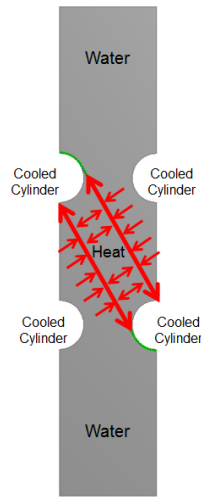


Figure 2. 3 Mechanism of enhanced heat transfer

However, due to the new application of thin layer ring (J. Xie 2013), the results shows that ice generated area in the storage tank can be increased when using the thin layer ring structure during the same charging period, since cooling energy can be transferred from water to the cooled cylinder through the thin layer ring more efficiently. The novel thin layer ring is used as extended fin to induce energy from not completely cooled region to the cooled cylinder. The mechanism of enhanced heat transfer is illustrated in Figure 2.3. The more detailed information will be discussed in the next chapter.

Based on previous research of heat transfer enhancement in thermal storage systems, the study mainly focused on investigating the heat transfer characteristics during the ice formation process in rectangular ITS tanks. In this study, a new structure of the thin layer ring is designed and employed to enhance the heat transfer performance in the ice thermal storage system, meanwhile

with foci on the effects of material, thickness, and arrangement of the thin layer ring on the overall enhancement of ice formation process.

2.4 Battery energy storage

Recently, in the application of battery energy storage, it has a more important and critical role in addressing many challenges beyond its historical role as a backup power source in the green buildings. It can also help address the increasing need for utilities to upgrade their investments in generation, transmission and distribution services to meet these challenges. Moreover, battery energy storage has been mainly integrated in electricity generation by PV. Since PV devices are the fastest growing renewable category with a 60% growth rate, followed by wind power at 27% and biofuels at 18% (Bortolini, Gamberi et al. 2014), battery energy storage also has a big market for the clean energy supply. Among all types of batteries, Li-ion batteries currently dominate the whole battery market in battery energy storage (Sarah Lichtner 2010). Meanwhile, pouch cell as a single unit in the battery package is a preferred power source for electric power source (Karimi and Dehghan 2014) and dominates 84% of the market (De-Leon 2010). Nowadays, most used EV batteries are remanufactured for the second use in the building energy storage. Due to the same operational mechanism in the EV application, stability and safety are also the most usually technical obstacles challenging the overall performance of battery energy storage system (BESS) (Lu, Han et al. 2013). In order to make BESS more stable and safe, recent research is more focused on using stable electrode materials (Yang, Bang et al. 2005) or improved thermal management system. In BESS, temperature increase has two different effects on the battery performance to meet the building energy demand. The beneficial effect is that BESS can work more efficiently to supply

enough electric demand as needed, but the unfavorable effect is that it can result in battery degradation, capacity reduction, fire and explosion, which is even more dangerous to the people in the building-scale application (Mohammadian and Zhang 2015). Therefore, thermal management system in BESS plays the most important role of safe operation and better performance. In this study, a novel structure is investigated as an active cooling method to improve heat transfer performance in BESS, since active cooling usually has the advantages of simple structure, light weight, low cost, easy maintenance and repair in the battery storage (Pesaran 2006, Mahamud and Park 2011, Giuliano, Prasad et al. 2012, Karimi and Li 2013, Park 2013, Xu and He 2013, Xun, Liu et al. 2013, Choi and Kang 2014).

As discussed above, among all types of batteries, Li-ion batteries currently dominate the whole battery market in battery energy storage (Sarah Lichtner 2010). Meanwhile, pouch cell as a single unit in the battery package is a preferred power source for electric power source (Karimi and Dehghan 2014) and dominates 84% of the market (De-Leon 2010). Most battery energy storage systems adopt the second-use Li-ion pouch cell as a single unit of battery package. Therefore, the temperature control during the operation is important to make battery work more efficiently and prevent BESS from fast battery degradation, capacity reduction, fire and explosion.

2.4.1 Current studies of BESS thermal performance improvement

In order to assure that thermal management system of BESS be able to control the operation temperature in the optimal range and eliminate the non-uniform cell temperature in the battery

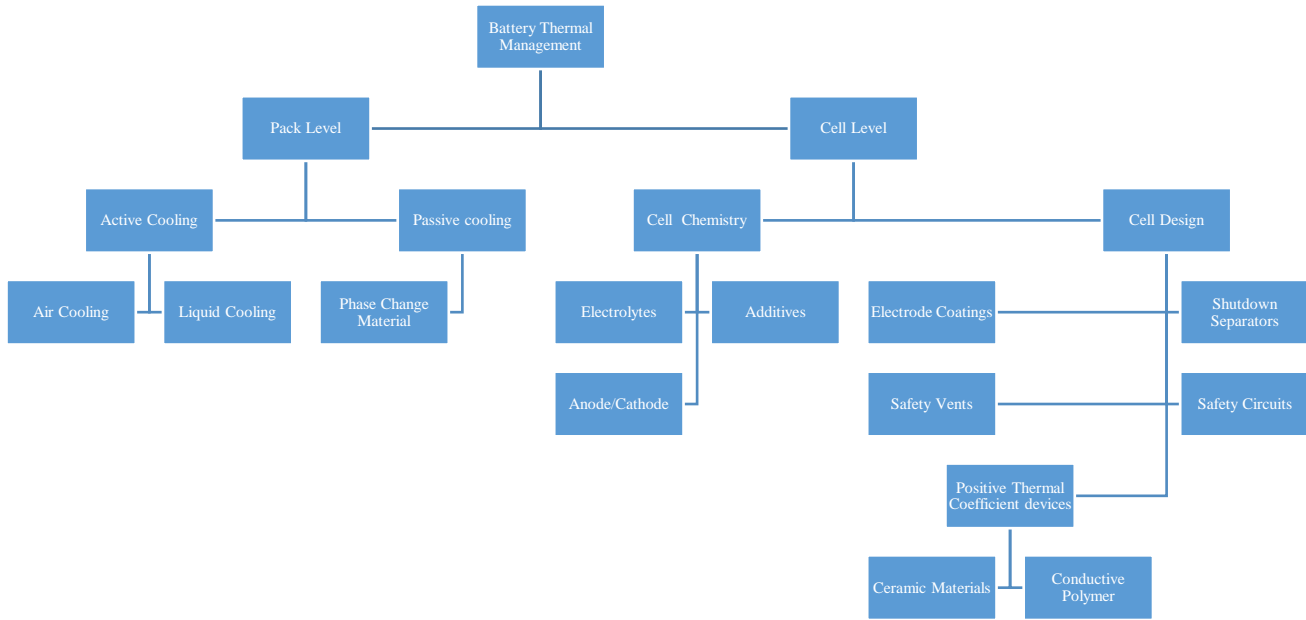


Figure 2. 4 Different levels of battery thermal management

pack, battery thermal management has become a very active research focus in recent years. These research focuses are being made on different levels shown in Figure 2.4. However, our study is focused on the pack level with air-side active cooling using vortex generation technique, since active cooling usually has the advantages of simply structure, light weight, low cost, easy maintenance and repair in the battery storage (Pesaran 2006, Mahamud and Park 2011, Giuliano, Prasad et al. 2012, Karimi and Li 2013, Park 2013, Xu and He 2013, Xun, Liu et al. 2013, Choi and Kang 2014). research to find the optimal cooling design of battery stack (Chen, Gao et al.

2003). As of now, a lot of research have been conducted to address thermal issues for LIB that continues to be considered as a clean, efficient, and environmentally responsible power source. Active cooling for LIB battery has been widely studied. In Choi and Kang's research, they developed a numerical thermal management system model with an active air cooling method (Choi and Kang 2014). A pack of single pouch cells is cooled by air flow passing through a channel between each single unit. Their model is useful for simulating the flow system and can be used to determine the appropriate cooling capacity for a specified design of the battery thermal management system. Fan, Khodadadi and Pesaran also developed a numerical model of thermal management in an air-cooled LIB module and experimentally validated their model (Fan, Khodadadi et al. 2013). Fan's model predicts that temperature rise in such a battery storage system can be lowered by reducing gap spacing between neighboring cells. It also indicates that the high flow rate of coolant can improve uniformity of battery temperature. Sun, Wang, Tossan and Dixon also conducted numerical research on thermal and electrochemical coupled cell modelling, considering the interaction between cell units (Sun, Wang et al. 2012).

Recently, cooling plates deployed on the battery surface have become the most common way to enhance heat transfer in the battery thermal management system. Smith et al. have studied the thermal effect of coolant flow rate and inlet temperature in a cooling plate, and their findings have improved the design guidelines for cooling plates to optimize battery thermal management systems (Smith, Hinterberger et al. 2014). Besides it, the battery thermal management using a mini-channel cold plate on the surface of each pouch cell was proposed by Huo and coworkers (Huo, Rao et al. 2015). Their research results show that the maximum battery temperature

decreases with an increase in the number of mini-channels and inlet mass flow rate, which is useful for the design of cold plate-based battery thermal management systems with a mini-channel structure.

Moreover, other researchers have proposed some new designs for battery thermal management systems. In Fathabadi's paper, he proposed a design to include several distributed thin ducts as a cooling media between batteries. His research results show batteries can achieve ultra-uniform voltage and temperature distributions and minimum temperature dispersion in each battery unit (Fathabadi 2014). Jarrett and Kin also investigated the thermal performance of a cooling plate applied on the surface of a battery (Jarrett and Kim 2011). They numerically studied thermal performance by changing the geometry of a cooling plate with internal channels through which a coolant is pumped. Their results indicate that a single cooling plate has good results in both pressure and temperature criteria as temperature remains uniformity. Chen et al. adopted a numerical method with different configurations of cooling plates in their research to find the optimal cooling design of a battery stack (Chen, Gao et al. 2003). Their research results show that a Serpentine-type cooling configuration has a better cooling effect than parallel-type configurations of cooling plates.

Battery configuring in such a way that battery cells operate in controlled temperature ranges is desirable. The goal of battery thermal management system is to increase the lifetime of lithium-ion cells by regulating the temperature influences on each cell. Maintaining temperatures between approximately range while achieving a uniform temperature within each cell helps limit battery

aging. Pesaran et al. have shown on the example of a pouch cell's placement that large temperature gradients over a single cell reduces its lifetime when this single cell is placed with one-side cooling (Fan, Khodadadi et al. 2013). The way with two-side cooling on each single cell usually is effective to regulate the temperature influences and extend the battery life.

2.4.2 Fin-like vortex structure to improve BESS thermal performance

In our study, vortex generation technique is adopted to enhance heat transfer performance on the surface of single pouch cell in BESS. Due to the high effectiveness and ease of implementation, it has emerged as a promising method for air-side active cooling enhancement and been used successfully in air-condition (Joardar and Jacobi 2008) and refrigeration applications (Sommers and Jacobi 2005). In this method, wing-like vortex generators are either punched or mounted on the heat-transfer surface to generate longitudinal vortices. As the vortices are advected downstream by the main flow in Figure 2.5 (1998), they cause bulk fluid mixing, boundary-layer modification and flow destabilization, thus improving convective heat transfer on the surface. However, the performance of this technique applied on the surface of pouch cell in BESS is still unknown, since heat generation inside the battery is complicated with electrochemical reaction heat, ohmic heat and entropic heat, which greatly impacts the temperature distribution on the cell surface and cooling effectiveness of thermal management system in BESS. Interaction mechanisms and detailed flow structure induced by vortex generator remain unclear in BESS application. It is also anticipated that the thermal-hydraulic performance could be further improved through optimization of vortex generator (VG) and placement on the surface of pouch cell in BESS.

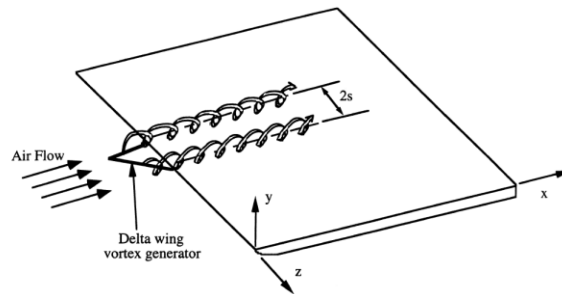


Figure 2. 5 A schematic showing the longitudinal vortices generated by a delta wing

2.5 Vortex generator technique

There are many kinds of vortex generators (VGs) that have been investigated. Some have been studied and used in industries for many years, and some have just been proposed as new design and their potential performance need to be further examined. In this section, a review of the most analyzed VG geometries will be conducted.

2.5.1 Delta winglet

Delta winglet is the most widely investigated and used VG geometry. To the author's knowledge, the first archival article on the heat transfer impact of VGs appeared in 1969 . Its authors, Johnson and Joubert, experimentally studied a circular cylinder in cross flow with delta winglet VGs located at a fixed angular position on the cylinder. It was shown that the local Nusselt number was increased by as much as 200% when using VG, but overall heat transfer results were not

encouraging due to decreases elsewhere on the cylinder. The enhanced thermal mixing caused local heat transfer enhancements.

In 1989, Fiebig and coworkers numerically investigated delta winglet performance in laminar channel flows (Fiebig, Brockmeier et al. 1989). In their research, it was observed that delta winglet pair generated counter-rotating longitudinal vortices, which showed an elliptic deformation, a wake-like axial velocity distribution in the core, and an absence of breakdown even at angles of attack as large as 50° . The spiraling motion caused by these vortices in the channel locally enhanced the heat transfer coefficient by a factor of 3 compared to its value in a wingless channel.

In 1992, Tiggelbeck and coworkers (Tiggelbeck, Mitra et al. 1992) experimentally studied the flow structure and heat transfer enhancement in plane channels built by parallel plates in transitional flow regimes. There were two rows of delta winglet VGs punched out of the channel wall. The experiments showed that the flow structure in the wake of the second row was qualitatively similar to that of the first row. The peak value of the span-averaged Nusselt number at the wake of the second row was strongly dependent on the spacing between the two rows. The vortices in the wake of the second row became more unsteady than the first-row vortices. Local heat transfer enhancement at the second-row VG was significantly higher than at the first row, and it was believed to be due to a booster effect of the second-row winglets on the oncoming vertical flow. Local heat transfer enhancements up to 460% were observed, and the enhancement appeared to increase with increasing Reynolds number. Following this work, Tiggelbeck et al. (Tiggelbeck,

Mitra et al. 1993) reported that aligned delta winglet double rows caused higher heat transfer enhancement than staggered double rows did. Heat transfer enhancements of 80% and drag increases of 160% had been found on wall areas 40 times the winglet area. The overall performance (ratio of heat transfer and drag increases) grew with increasing Reynolds number. Furthermore, Ferrouillat et al. (Ferrouillat, Tochon et al. 2006) found that heat transfer and mixing efficiency were optimum when distance between VG rows were around 7-10 times channel height. Their numerical study also showed that for heat exchanger applications, unsteady computation with a large number of time steps provided no extra information, since the vortices generated were almost steady. In a paper by Wu and Tao et al. (Wu and Tao 2007), 3-D numerical simulation results were presented for laminar flow heat transfer in a fin-and-tube heat exchanger with VGs on its surface. The effects of Reynolds number (from 800 to 2000) and attack angle (30° and 45°) of multi-row delta winglet VGs were examined. The numerical results were analyzed from the viewpoint of field synergy principle, which could cause flow interaction significantly. Heat transfer enhancement of delta winglet with an attack angle of 45° was larger than that of 30° . However, pressure drop for the delta winglet with 45° attack angle was about 10-12% higher than that for the plain-plate heat exchanger, while pressure drop with 30° attack angle was even 8-10% lower. From this point of view, the delta winglet pairs with attack angle of 30° were more effective than delta winglet pairs with attack angle of 45° , especially under higher Reynolds numbers. In 2009, Chu et al. (Chu, He et al. 2009) numerically studied fin-and-oval-tube heat exchangers with delta winglets. For Reynolds number ranged from 500 to 2500, it was found that the average Nusselt number increased by 13.6-32.9% over the baseline case and the corresponding pressure loss increased by 29.2-40.6%. The results were also analyzed on the basis of field synergy principle.

The VGs with placement of downstream, angle of attack $\alpha = 30^\circ$ and minimum tube-row number displayed the best heat transfer performance.

Some research has been conducted on delta-winglet VG configurations, such as "common flow up" and "common flow down". In 2002, Torii et al. (Torii, Kwak et al. 2002) conducted the first experiment with delta winglets arranged as a "common flow up" configuration. They analyzed two arrangements of tube banks in the range of Reynolds number from 350 to 2100. Heat transfer was augmented by 30% to 10% and pressure loss was reduced by 55% to 34% in the case of staggered tube banks, while heat transfer was augmented by 20% to 10% together with a pressure loss reduction of 15% to 8% in the case of in-line tube banks. After this research, Tian and his coworkers numerically studied fluid flow and heat transfer in a flat-plate channel with delta winglets (Tian, He et al. 2009). They analyzed "common flow up" and "common flow down" configurations and concluded that "common flow down" and "common flow up" had almost the same overall performance when delta winglets were used for heat exchangers, while the friction factor of a single channel with "common flow up" configuration was larger than that of "common flow down" configuration.

Delta winglet mounted on both sides of fin surfaces obtained satisfactory heat transfer enhancement (Song, Wang et al. 2008). Using this arrangement, the height of VGs could be reduced, and the pressure drop was also reduced. The study revealed that if VGs on one surface of the fin was determined, the locations where VGs were mounted on the other surface were very

important and it depended on the value of Reynolds number. In 2009, Tian and coworkers conducted a comparative study on the air-side performance of wavy fin-and-tube heat exchangers with punched delta winglets in staggered and in-line arrangements (Tian, He et al. 2009). Compared with the wavy fin baseline, the j and f factors with delta winglets in staggered and in-line arrays were increased by 13.1%, 7.0% and 15.4%, 10.5% at $Re = 3000$, respectively. From recent research by Lei et al. (Lei, He et al. 2010), the results showed that the delta winglet VGs with an attack angle of 20° and an aspect ratio of 2 provided the best overall performance over the range of Reynolds number computed. The optimal configuration was shown to increase Colburn j factor by 35.1-45.2% with a corresponding increase of 19.3-34.5% in the friction factor.

Followings are VG arrays investigated recently. In 2007, Jacobi and Joardar (Joardar and Jacobi 2006) conducted a numerical study on flow and heat transfer enhancement using an array of delta winglet VGs in a fin-and-tube heat exchanger. The results showed that the 3VG-inline-array configuration achieved enhancements up to 32% in total heat flux and 74% in j factor over the baseline case, with an associated pressure-drop increase of about 41% when Re was 850 with constant tube-wall temperature boundary conditions. Following this work, Joardar and Jacobi experimentally investigated VG array performance in compact plain-fin-and-tube heat exchangers (Joardar and Jacobi 2008). They reported that the air-side heat transfer coefficient increased from 16.5% to 44% for a single-row winglet arrangement with an increase in pressure drop of less than 12%. For a three-row VG array, the enhancement in heat transfer coefficient increased from 29.9% at $Re = 960$ to 68.8% at $Re = 220$ with a pressure drop penalty from 26% to 87.5%. From the results, it could be determined that VG arrays can significantly enhance the performance of fin-

tube heat exchangers with flow depths and fin densities typical to those used in air-cooling and refrigeration applications.

2.5.2 Delta wing

Delta wing VG is also popularly investigated and used in industries. In 1989, Biswas et al. (Biswas, Mitra et al. 1989) numerically analyzed laminar mixed convection flows and heat transfer in a rectangular channel with a delta wing mounted on the bottom wall. The heat transfer enhancement between the stream and the channel wall was well evidenced. The augmentation was explained to be primarily due to longitudinal vortices generated by the wing. From Fiebig and coworkers' research in 1991 (Fiebig, Kallweit et al. 1991), The results showed that local heat transfer augmentation of several hundred percent and mean heat transfer enhancement of more than 50% over an area more than 50 times the VG area where achieved.

In 1992, Biswas and coworkers (Biswas and Chattopadhyay 1992) conducted another numerical study on heat transfer in a channel with built-in wing-type VGs. It was found that downstream velocity magnitudes for the case with wing-type VGs punched out from wall surface were smaller than those for the case without stamping. For the situation with VGs punched, fluid got entrained through the holes underneath the wings and there was loss of fluid through the holes. In their results, spanwise average Nusselt number showed increases as large as 34% even at the exit of a long channel with an angle of attack of 26° . Jacobi and Joardar (Joardar and Jacobi 2005) conducted experimental study under both dry-and wet-surface conditions for a delta wing vortex-

enhanced louvered-fin heat exchanger. The results showed that average heat transfer increase over baseline case of 21% for dry conditions and 23.4% for wet conditions were achieved with a pressure drop penalty smaller than 7%. In the meantime, Jacobi and Sommers (Sommers and Jacobi 2005) studied air-side heat transfer enhancement of a refrigerator evaporator using delta wing VGs. In their study, for air-side Reynolds number between 500 and 1300, the air-side thermal resistance was reduced by 35-42% when VGs were used. Correspondingly, the heat transfer coefficient was observed to range from 33 to 53 W/m²K for the enhanced heat exchanger and from 18 to 26 W/m²K for the baseline heat exchanger.

2.5.3 Rectangular winglet

Rectangular winglet was numerically investigated by Sohankar and Davidson (Davidson 2001). Their results showed that the flow was steady up to $Re = 1000$ and that unsteady flow occurred at a higher Reynolds number, for all cases in which the convective term was discretized by central differencing. However, the flow showed steadiness for all Reynolds numbers when the QUICK (Quadratic Upwind Interpolation of Convective Kinematics) scheme was used. They also found that a rectangular winglet VG generates longitudinal vortices behind the VG, which enhanced heat transfer locally and globally by their corkscrew motions. These vortices induced a downwash flow toward the heat transfer surface, which enhanced the mixing of cold and hot fluid. In 2004, experiments conducted by Leu and coworkers (Leu, Wu et al. 2004) showed that the implementation of rectangular winglets was able to improve heat transfer performance in the wake regions for Reynolds numbers from 400 to 3000. Their visual and numerical results demonstrated that this kind of VGs not only produced longitudinal vortices, but also aided the fluid into the wake

re-circulation zone. As the span angle α was increased, strength of the longitudinal vortexes was intensified and both j and f factors increased. The arrangement of VGs with a 45° attack angle provided the relative best heat transfer enhancement with a 8-30% increase in j factor across the Re range, while f factor only increased by 11-15%. A reduction in fin area of 25% may be obtained if these VGs were used on plain fins at $Re = 500$. In Chu and coworkers' research (Chu, He et al. 2009), they studied three enhancing configurations which were inline-1RWP (Rectangular Winglet Pair) case, inline-3RWP case, and inline-7RWP case. It was found that air-side heat transfer coefficient improved by 28.1-43.9%, 71.3-87.6%, and 98.9-131% for these three enhancing configurations, accompanying with pressure drop penalty increase of 11.3-25.1%, 54.4-72%, and 88.8-121.4%, respectively.

2.5.4 Impact of different parameters

Winglets caused higher heat transfer enhancement than wings for otherwise identical parameters and thus were more effective than wings (Fiebig 1998) (Fiebig 1995). In terms of flow structure, the main difference between the flow fields with wings and with winglets was that wings could not generate trailing edge wakes. The vortices generated by delta winglets had divergent axes and strongly elliptical cross-sections. However, in Fiebig and coworkers' study (Fiebig, Kallweit et al. 1991), the heat transfer enhancement per unit VG area was shown to be highest for wings followed by winglets.

According to the performance evaluation parameter, $(Nu/Nu_0)/(f/f_0)$, the channel with delta winglet had better overall performance than rectangular winglet (Tian, He et al. 2009) (Zhu, Fiebig et al. 1993). At the same time, delta winglet VGs was more efficient than rectangular winglet VGs in terms of compactness criterion (Ferrouillat, Tochon et al. 2006). However, delta and rectangular winglets gave similar performance if all other dimensionless parameters were the same. Delta winglet VGs were more effective per unit VG area for heat transfer enhancement than rectangular winglet VGs. From Table 2.1 (Zhu, Mitra et al. 1993), delta winglet showed to be the best heat transfer performance. However, the ratio of heat transfer enhancement to flow loss increased suggesting better performance of the rectangular winglet pair than of other forms of VGs in a turbulent channel flow.

Table 2. 1 Comparison of global effects of four VGs

Comparison of global effects of the four vortex generators on heat transfer and flow losses in turbulent channel flow: $T_w = 2T_0$, $A_L/A_w = 30$, $\beta = 25$, $Re = 50000$, $Pr = 0.7$

	Nu_m/Nu_{om} upper wall	Nu_m/Nu_{om} lower wall	Nu_m/Nu_{om} average for both walls	C_{fm}/C_{f0}
DWP	1.20	1.18	1.19	4.2
RWP	1.24	1.10	1.17	4.0
DW	1.25	1.08	1.165	5.1
RW	1.28	1.04	1.16	4.9

$Nu_{om} = 230$; $C_{f0} = 4.6 \times 10^{-3}$.

Table 1. Comparison of global effects of the four VGs (DWP: delta winglet pair; RWP: rectangular winglet pair; DW: delta wing; RW: rectangular wing) on heat transfer and flow losses in turbulent channel flow (Zhu, Mitra et al. 1993)

When thicker VGs were used, stronger and bigger streamwise vortices were formed downstream of the VGs, which gave rise to higher Nusselt numbers. Similar global results were found when using thicker VGs with a lower angle of incidence as when using thin VGs with a higher angle of incidence (Davidson 2001). However, thicker VGs were more useful for low and moderate Reynolds number (Zhu, Fiebig et al. 1993).

The “common flow up” and “common flow down” configurations of delta winglets had almost the same overall performance. For the rectangular winglets, the “common flow down” configuration had a better overall performance than the “common flow up” configuration, because the friction factor of the channel with “common flow down” configuration was smaller than that of “common flow up” configuration (Tian, He et al. 2009).

As suggested by Fiebig's study (Fiebig 1998), longitudinal vortices enhanced heat transfer locally and globally by their corkscrew motion and were very persistent in both laminar and turbulent flows. For laminar flow, the heat transfer enhancement increased with increasing Reynolds number.

From Table 2.1 (Zhu, Mitra et al. 1993), delta winglet should be the better choice, otherwise delta wing, rectangular wing or rectangular winglet may be more suitable. The flow losses are however 4-5 times larger than that without vortex generator. So, the ratios of heat transfer enhancement to flow loss increase suggest better performance of the rectangular winglet pair than of other forms of VGs in a turbulent channel flow.

The CFU and CFD configurations of delta winglet have almost the same overall performance. For the rectangular winglet, the CFD configuration has a better overall performance than the CFU configuration. The friction factor of the channel with CFU configuration is larger than that of CFD configuration (Tian, He et al. 2009).

In Fiebig's study (Fiebig 1998), Longitudinal vortices enhance heat transfer locally and globally already in steady flow by their corkscrew motion and are very persistent in laminar and turbulent high Re flows. For laminar flow, the heat transfer enhancement increase with increasing Re.

The past research has revealed that increased mixing of the freestream fluid with the boundary layer fluid usually leads to greater heat transfer enhancement. Streamwise longitudinal vortices and spanwise vortex shedding can dramatically improve fluid mixing and thus enhance heat transfer. It is natural to expect that applying streamwise vortices to VG could create vigorous fluid mixing and generate higher heat transfer enhancement. Unfortunately, to date there has been even no research on applying VG on the surface of single cell in BESS. The research proposed here seeks the heat transfer enhancement in BESS with new configurations and arrangements of VG. Flow structure and heat transfer enhancement will be studied together.

2.5.5 Summary of vortex generator

The past research has revealed that streamwise longitudinal vortices and spanwise vortex shedding can dramatically improve fluid mixing and thus enhance heat transfer. However, to date there has

been no numerical study on vortex generators deployed in a V-formation. Interaction mechanisms of vortices generated by different VGs remain unclear at this stage, and its impact on heat transfer behavior is also unknown. In order to mimic group formed movement of animals in nature and utilize these favorable interactions in human fluid-flow technology, the research proposed here seeks to investigate detailed flow structure and attendant heat transfer enhancement induced by the novel arrangement. The impact of different parameters on the performance will also be studied to provide design guidelines for better implementation of this technology.

Nowadays, vortex generation technique is a new way to address thermal issues in battery cell. This technique can increase local heat transfer enhancements up to 460% were observed by mixing bulk fluid, modifying boundary-layer and destabilizing flow, thus improve convective heat transfer. Usually, it is reported that up to 80% heat transfer enhancement can be achieved in laminar flow in which fluid flows stably over heat transfer surface, and more than 80% achieved in turbulent flow in which fluid flows unstably over the heat transfer surface (Wu and Tao 2007, Joardar and Jacobi 2008, Chang, Wang et al. 2009, Chu, He et al. 2009, Tian, He et al. 2009, Lei, He et al. 2010). Vortex generation technique can also be applied within micro channels to enhance heat transfer (Wang, Chen et al. 2007, Liu, Teng et al. 2011, Chen, Teng et al. 2014), so the surface of a pouch cell is large enough for the application of this technique. Currently, there are four types of vortex generators used for local heat transfer enhancement (Chu, He et al. 2009). Studies have shown that winglets caused higher heat transfer enhancement than wings, so they are more effective than wings. In terms of flow structure, the main difference between the flow fields with

wings and with winglets is that wings could not generate trailing edge wakes (Fiebig 1995, Fiebig 1998). Therefore, delta winglet and rectangular winglet are adopted in this study.

2.6 Taguchi method

Here the Taguchi method is adopted to numerically evaluate the performance of thin layer ring for thermal enhancement in ITS system statistically and comprehensively.

The Taguchi method is a methodology for the application of designed experiments. It is developed by Dr. Taguchi, the “father of robust design”. His method can make experiment simpler by using fewer experimental designs and providing a better understanding of the variations of system. The method advocates a three-stage design methodology for:

1. Designing products/processes so as to be robust to environmental conditions;
2. Designing and developing products/processes so as to be robust to component variation;
3. Minimizing variation around a target value;

Many optimal robust designs of a product or process have been investigated with Taguchi method. His optimization method can be characterized as a three-step approach, which includes system design, parameter design, and tolerance design.

In system design, it contains product design and relative process design. As discussed in product design, it includes the selection of materials, components, tentative product parameter values, etc.

In parameter design, it is used to optimize the characters of the product parameter values. The

optimal product parameter values obtained from the parameter design are not sensitive to the variation of environmental conditions and other noise factors. Therefore, the parameter design is the most important step among three steps of the Taguchi method. In fact, Fisher developed the classical parameter design that is complex and cannot be easily used. When the number of product parameters increases, a large number of experiments should have to be carried out. However, the Taguchi method contains a special design of orthogonal arrays to analyse the entire parameter space with a small number of experiments.

Usually, the parameter design of Taguchi method to find the optimal combination of product contains the following steps, each step will be presented in details for the parametric study of thin layer ring below:

- Identify the performance characteristics and select product parameters to be evaluated.
- Determine the number of levels for the process parameters and possible interactions between product parameters.
- Select the appropriate orthogonal array and assignment of product parameters to the orthogonal array.
- Conduct the experiments based on the arrangement of the orthogonal array.
- Calculate the S/N ratio.
- Analyse the experimental results using the S/N ratio.
- Select the optimal levels of process parameters.
- Verify the optimal process parameters through the confirmation experiment.

CHAPTER 3 NUMIERICAL STUDY OF THIN LAYER RING IN THERMAL ENERGY STORAGE SYSTEM

3.1 Introduction

In this chapter, a numerical model is developed to simulate the ice formation in a typical ice thermal storage system. The study is proposed mainly to investigate the heat transfer characteristics during the ice formation process in rectangular TES tanks. In this study, a new structure of the thin layer ring is designed and employed to enhance the heat transfer performance in the ice thermal storage system, meanwhile with foci on the effects of material, thickness, and arrangement of the thin layer ring on the overall enhancement of ice formation process. The Taguchi method is introduced into this study for optimization and the database will also be obtained by numerical method. The analytical results will provide quantitative information on various design parameters affecting the thin layer ring performance, and based on that, the main factors could be selected for optimal design. The optimal design value of each parameter will be useful for future improving of the TES system.

3.2 Model description

3.2.1 Physical model

The investigated area of this study is the cooled cylinder in the fixed rectangular space. The physical geometry of an ITS tank and the analyzed rectangular space is shown in Figure 3.1. The cross section of the ITS tank is shown on the left. Many circular tubes represent the cross section

of refrigeration cylinders. In the middle, the enlarged section shows the configuration of these refrigeration cylinders in details. During the solidification of water, ice can be generated gradually from the outer surface of cylinders. Since both cylinder and water condition on one side are equivalent to the opposite side in the analysed space marked with red color, the boundary conditions on both red lines are equivalently axisymmetric. Therefore, the rectangular area marked with red color can be representative to other areas with the same conditions in the ITS tank. To validate the numerical model, one cooled cylinder was considered at first, but solidification (ice formation) around the four cylinders in a fixed volume was studied to understand the interactive effect of the neighbouring cylinders (Figure 3.1). According to the experimental research on solidification presented in the literature (Sasaguchi, Kusano et al. 1997), dimensions of the investigated geometry were kept the same to compare the experimental result with the numerical result in this study. Therefore, the diameter of the cylinder was set as d ($d=0.0254\text{m}$), and rectangular space heights (L) was taken as $7d$ and $10d$. Longitudinal and transverse spacing were $2d$ for both geometries. Detailed parameters are presented in Figure 3.2 and Table 3.1.

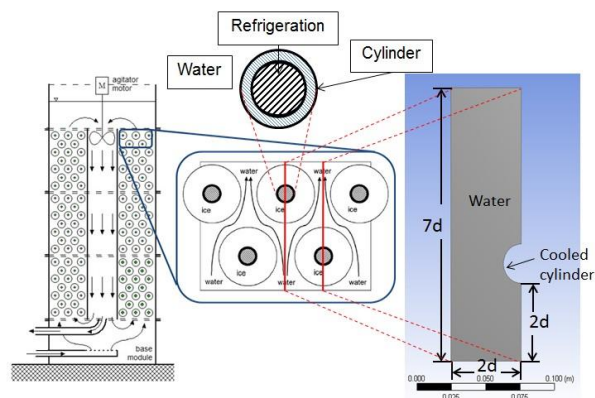


Figure 3. 1 Geometry of the ITS tank (Left) and the analyzed rectangular space

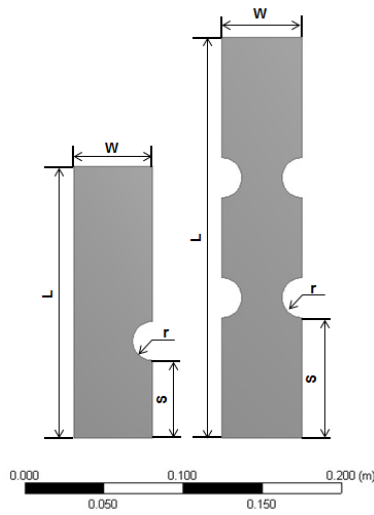


Figure 3. 2 One cylinder and four cylinders rectangular space

Table 3. 1 Dimensions of analyzed space

Parameter (unit)	One cylinder	Four Cylinder
W (m)	0.0508	0.0508
L (m)	0.1778	0.254
S (m)	0.0508	0.0762
r (m)	0.0127	0.0127

3.2.2 Governing equations

All numerical studies were carried out based on the condition of transient natural convection in water with the cooled cylinder. The FLUENT program with a finite volume method was used to solve ice formation in fixed rectangular space as one and four cylinder geometries. In order to study the transport phenomena during solidification, an enthalpy formulation based approach was

chosen within FLUENT. The governing equations involved in numerical modeling are listed below.

Continuity equation:

$$\frac{\partial \rho}{\partial t} + \nabla \cdot (\rho V) = 0 \quad (3.1)$$

Momentum equation:

x-Momentum:

$$\frac{\partial}{\partial t}(\rho u) + \nabla \cdot (\rho u V) = -\frac{\partial P}{\partial x} - \frac{\mu}{k} u + \nabla \cdot (\mu \nabla u) \quad (3.2)$$

y-Momentum:

$$\frac{\partial}{\partial t}(\rho v) + \nabla \cdot (\rho v V) = -\frac{\partial P}{\partial y} - \frac{\mu}{k} v + \nabla \cdot (\mu \nabla v) + (\rho_m - \rho) g \quad (3.3)$$

Energy equation:

$$\frac{\partial}{\partial t}(\rho h) + \nabla \cdot (\rho h V) = \nabla \cdot \left(\frac{k}{c} \nabla h \right) - \frac{\partial}{\partial t}(\rho \beta L) - \nabla \cdot (\rho \beta L V) \quad (3.4)$$

Where t is time; ρ is density; P is pressure; V is velocity vector; u and v are velocity components in x and y directions; μ is dynamic viscosity; β is liquid volume fraction; L is latent heat.

For the mushy zone during phase changing, Darcy's law and the Kozeny-Carman equation were taken into consideration.

Kozeny-Carman equation:

$$K = K_0 \left(\frac{\beta^3}{(1-\beta)^2} \right) \quad (3.5)$$

Sensible enthalpy-temperature relation,

$$h = \begin{cases} C_s T & T < T_f \\ C_l T & T \geq T_f \end{cases} \quad (3.6)$$

Where K_0 is empirical constant in Kozeny-Carman equation shown below; K is permeability; T_f is fusion temperature; C_s and C_l are specific heats for solid and liquid phases, respectively.

In the energy equations shown above, sensible enthalpy, h , is defined by following equation.

$$h = h_{ref} + \int_{T_{ref}}^T c dT \quad (3.7)$$

Where, h_{ref} is reference enthalpy; T_{ref} is reference temperature; c is specific heat at constant pressure.

3.2.3 Boundary conditions

For simplicity, the water in the investigated space was considered as Newtonian (Egolf and Kauffeld 2005), incompressible, and laminar flow.

Boundary Conditions: Since the investigated rectangular space is symmetrical to the neighbouring space and no heat transfers through the top and bottom walls, the following assumptions are made for boundary conditions: (1) symmetry condition at left and right boundaries, except cylinder surfaces; (2) Adiabatic and no-slip conditions at top and bottom walls; (3) $h = h_w = C_s T_w$ and $u = v = 0$ at cylinder surfaces; (4) Perfect contact on cylinders.

Initial conditions: Since the refrigeration temperature inside cylinder is much colder than the temperature of water in the investigated space, the following assumptions were made for initial conditions: (1) Water is at rest at $t = 0$; (2) $h = h_i = C_l T_i$ at $t = 0$; (3) $t_c = 263.15\text{K}$ (temperature on the cylinder surface); (4) $t_w = 277.15\text{K}$ (temperature of water). Other thermal properties are shown in Table 3.2.

Table 3. 2 Thermo-physical properties of water in the study

Property	Specification	Property	Specification
ρ_f	999.833 kg/m ³	μ	$0.5712-0.005705T+1.91\times 10^{-5}T^2-2.141\times 10^{-8}T^3$ kg/m-s
c_s	2,217 j/kg-k	μ_f	0.00162 kg/m-s
c_l	4,180 j/kg-k	L	334,000 j/kg
K_s	1.918 m ²	T_f	273.15 K
K_l	0.578 m ²	K_0	10 ⁻⁸ m ²

3.2.4 Solution method and grid independence validation

A quadrilateral grid was used for the simulation, and a refined grid distribution was applied near cylinder surfaces for the accuracy of the numerical solution. Therefore, the region around the location where the cylinder was placed had a higher resolution, which can increase the accuracy of simulation around the cylinder surfaces. The created mesh for one and four cylinder cases is shown in Figure 3.3.

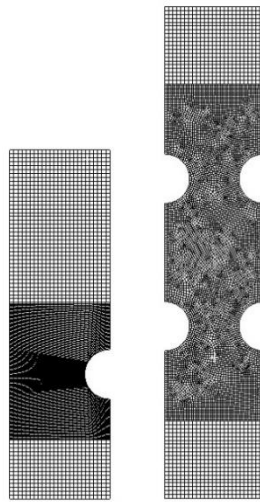


Figure 3. 3 Mesh distribution

To solve the equations presented in previous section, the SIMPLEC algorithm was used, while the governing equations for momentum and energy were discretized with finite volume formulation using the QUICK scheme. The gradient was Green-Gauss based. Considering the control of the convergence of solution, the under-relaxation factors were set as 0.3 and 0.7, respectively. The residuals of continuity, momentum, and energy equations were set to be less than 1×10^{-4} , 1×10^{-3}

and 1×10^{-8} , respectively. Based on the solution method described above, the iteration continued until the computation converged and became stable.

Since the mesh quality and grid numbers have significant impact on the accuracy of a solution, the validation of the solution of the grid number was addressed to test four different grid numbers which were 3,923, 15,668, 24,520 and 35,425. The ratio of A_i/A_c at 900 seconds along the solidification process with different grid number is shown in Figure 3.4. It can be seen that the

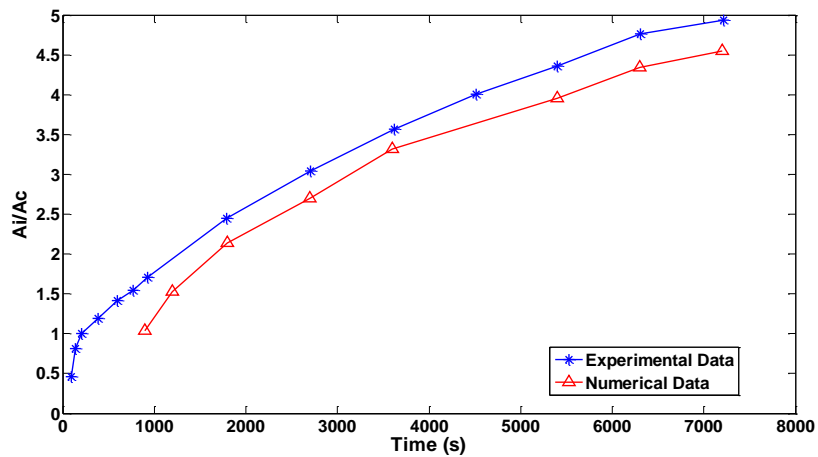


Figure 3. 4 Validation of numerical model

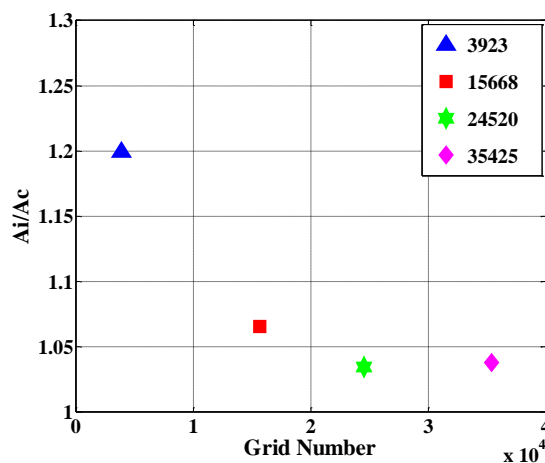


Figure 3. 5 Ratio of A_i/A_c with different grid number at 900s

ratio of A_i/A_c does not vary greatly and nearly remains a constant value (difference less than 5%) when the grid number is higher than 24,520. To ensure the accuracy of the computational solution, the grid number was created as large as 24,520 due to the approaching similarity of values.

To check the validity of the present numerical model, several validations were performed by comparing numerical data with the experimental data based on the same assumptions and conditions. As shown in Figure 3.5, the time-wise area ratio (A_i/A_c) matches well with experimental data in entire time range. From this promising result, it can be concluded that the numerical model created in this study is valid and can be used for ice formation with complicated scenarios.

3.3 Results and discussion of thin layer ring study in ITS system

3.3.1 Ice formation in one cylinder rectangular space

Calculations were carried out when one cylinder was placed near the bottom of the rectangular space. In Figure 3.6, the temperature distribution at time intervals of 900s, 1800s, 3600s and 7200s

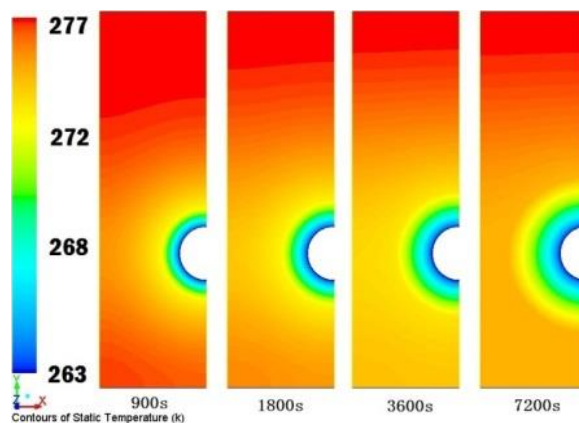


Figure 3. 6 Temperature distribution

can be observed. Since the temperature at the surface of the cooled cylinder was set below the solidus temperature of pure water (273.15 K), heat was taken from the water to the cylinder surface through natural convection within water. As a result, water was solidified after the temperature went below 273.15K. As time progresses, the water temperature in upper part of the rectangular cavity approached solidification temperature (273.15K). After 7200s, water temperature is nearly uniform in lower part of rectangular space, except around surface of cylinder.

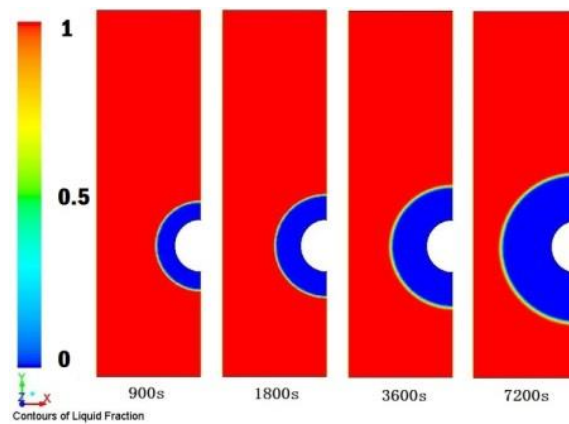


Figure 3. 7 Liquid fraction distribution

The solidified area presented in Figure 3.7 shows the liquid fraction in the investigated geometry. Due to the temperature being below the solidification temperature, the water was transformed into ice. In the results, liquid fraction below 1 represents a water-ice coexistence area. When the liquid fraction reduces to 0, water is solidified completely into ice. Consequently, a thermally layered region is gradually observed. At 7200s, the thickness of the ice layer is twice that of the diameter of the cylinder.

3.3.2 Ice formation in four cylinder rectangular space

In a typical ITS system, there are many cooled coils inside to freeze water for the ice thermal storage. During the ice formation process, there is a continuously changing cavity in the center of the rectangular geometry. In Figure 3.8, liquid fraction shows the cavity circled in orange gradually disappears when the water fully turns into ice. If water in the cavity changes to ice as quickly as the water around the cylinders does, the time period of ice formation can be shortened and the overall process would be efficient.

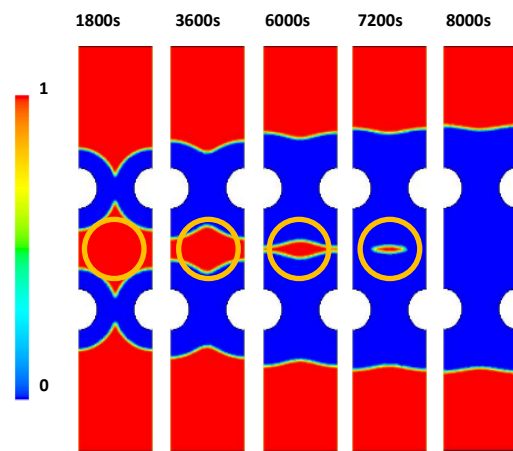


Figure 3. 8 Cavity during ice formation

In previous literature review, an increased heat transfer surface deployed inside the cylinder can enhance the heat transfer rate (E.M. Sparrow 1984, P.V. and M.V. 1986, Lacroix 1993). Therefore,

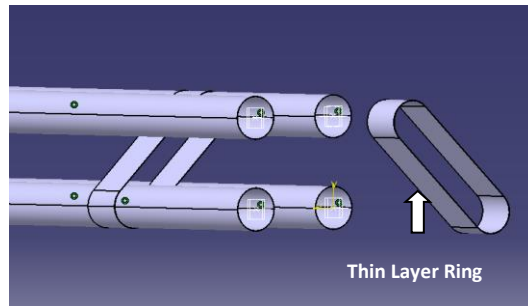


Figure 3. 9 3D geometry of thin layer ring

using a similar idea, heat in the cavity can be absorbed by the surface of the thin layer ring attached to the cylinder. The geometry of the 3D thin layer ring is shown in Figure 3.9. The material is initially set to be aluminium. To investigate its performance, a numerical model with the thin layer ring was built in FLUENT and the results were compared with the results without thin layer ring, these are presented in Figure 3.10. It is apparent that there is a cavity in the center of the case without the thin layer ring at 7200s. However, after using the thin layer ring, the cavity in the center disappeared at 7200s.

The enhanced heat transfer mechanism is shown in the schematic diagram (Figure 2.3). Heat in the center space is absorbed by the thin layer ring and transferred through it to the cooled cylinder surface by heat conduction. During this thermal process, the convective heat transfer could be efficiently achieved in water. Additionally, the heat transfer rate of the thermal conduction within the thin layer ring is dependent on the conductivity of the thin layer ring structure and material properties. The base line of the thin layer ring presented in Table 3.3 is applied to investigate the

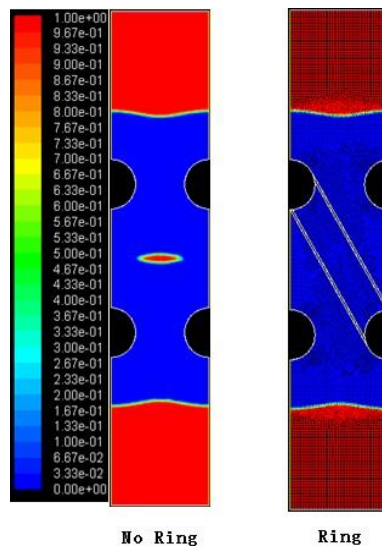


Figure 3. 10 Comparison of liquid fraction at 7200s

parametric impact on its performance. Further study of different scenarios of thin layer ring applications will be addressed in the next section. The results of each scenario will be compared with the base line.

Table 3. 3 Baseline of thin layer ring

Material	Thickness (mm)	Arrangement
Aluminium	1	Staggered

3.4 Factorial effect analysis on thermal performance

3.4.1 Heat transfer enhancement using thin layer ring

Using the thin layer ring in the ice storage tank, has been proved, from the computational results, that the time of the ice formation can be shortened and the area ratio can be increased. In other words, the overall efficiency of ice thermal storage system can be improved. However, there is a large arrangement space as well as different placement strategies which need to be investigated for the utilization of a thin layer ring for the improvement of an ice thermal storage system. This is to say, many unknown parameters and different arrangements should be explored and determined first. For this reason, material, thickness, and different placements were investigated for this thin layer ring structure. The parameters with different values in the following studies are shown in Table 3.4.

Table 3. 4 Investigated parameters

Parameter	Value				
Material	Aluminium	Copper	Stainless Steel	Magnesium Alloy	-
Thickness (mm)	0.25	0.5	1	2	3
Arrangement	Staggered	Parallel	-	-	-

3.4.2 Effect of material

In industrial fields, aluminium, copper, and stainless steel are the three most commonly used materials for heat transfer; meanwhile magnesium alloy has recently been applied to high-tech field as heat transfer material. Typically, stainless steel has the lowest thermal conductivity among these four, while aluminium is slightly higher than magnesium alloy. Copper has the best heat transfer performance among the four materials. In this study, these four materials were chosen for the thin layer ring, while the other parameters were kept the same. To fully analyze the ice formation process in the middle of the investigated rectangular space along with time, the temperature at the center point was monitored during the studies.

The results of liquid fraction and temperature distribution from different material cases are shown in Figure 3.11. On the left side, the copper case has the largest area of ice generated at 1800 seconds. On the second row of liquid fraction, water in the middle of the rectangular space formed into the ice completely with the aluminium and copper rings at 3600 seconds. On the third row of liquid fraction, water in all cases with the thin layer ring turned into ice at 7200 seconds, but ice

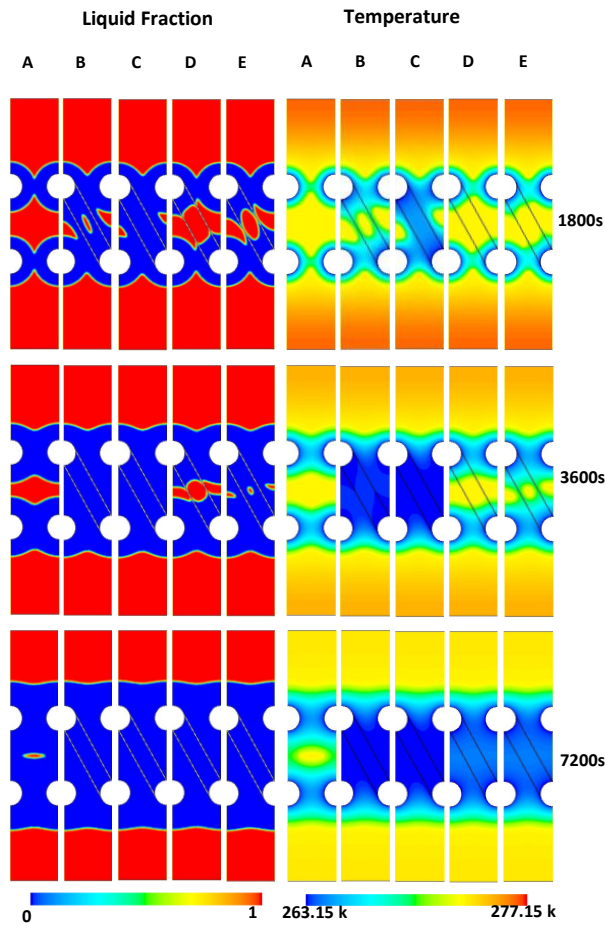


Figure 3. 11 Liquid fraction (left) Temperature (right)

A (without ring), B (Aluminum), C (Copper)

D (Stainless steel), E (Magnesium alloy)

formation at the center in the case without the thin layer ring didn't achieve completely. Moreover, temperature distribution on the right side shows that temperature gradient near the thin layer ring is relatively lower in the rectangular space. Temperature at the center was gradually approaching the freezing point for the case without the thin layer ring, but the rate of reaching the freezing point for the case with the thin layer ring is dependent on the material conductivity.

It can be seen, in Figure 3.12, that the temperature at the center of the rectangular space took nearly 500 seconds to reach the lower limit of the phase transition temperature (freezing point) for the copper case, 800 seconds for the aluminium case, 800's for magnesium alloy case, 1600 seconds for the stainless steel case and 2000 seconds for the case without the ring. After that, the temperature at the center point in five different cases remained constant during the phase transition of water from liquid to solid. At the start of the phase transition, heat transfer was primarily done by convection within the water region and by conduction after the water turned into ice. This occurred because during ice formation, the rate at which energy was absorbed from the refrigeration cylinder balanced the rate at which energy was transferred to the adjacent phase

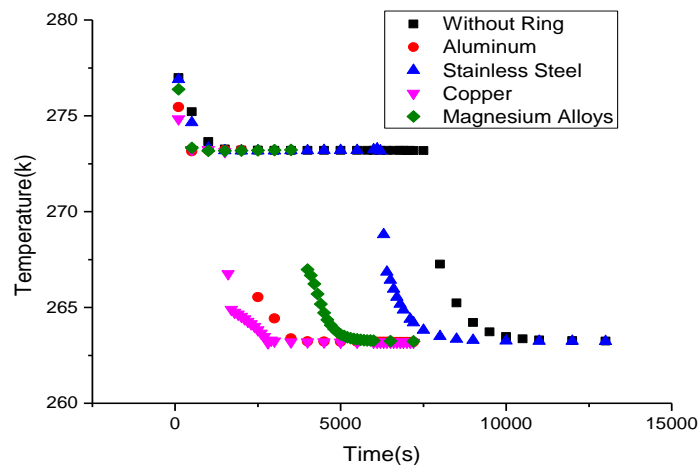


Figure 3. 12 Temperature variation in the middle vs. time

changing material as a result of the temperature gradient in the rectangular region. The latent heat transfer time is between 500 seconds to 1500 seconds in the copper case, between 800 seconds to 2200 seconds in the aluminium case, between 800 seconds to 3800 seconds in the magnesium alloy case, between 1600 seconds to 6200 seconds in the stainless steel case, between 2000 to 7500 seconds in the no ring case. A rapid drop of the phase transition temperature occurred from 7500 seconds in the case without the ring at the start of the sensible heat transfer process and continued changing until the temperature was close to the refrigeration temperature of 263.15K at 130000 seconds. A similar process also occurred from 6000 seconds to 9000 seconds in the stainless steel case, from 2200 to 4500 seconds in the aluminium case, from 3800 seconds to 7500 seconds in the magnesium alloy case, from 1500 seconds to 2800 seconds in the copper case.

3.4.3 Effect of thickness

Typically, with an increase in thickness, the thermal resistance will also increase, while the heat transfer rate will decrease due to the thermal conduction distance. In this study, the thicknesses of thin layer ring are evaluated at 0.25mm, 0.5 mm, 1 mm and 2 mm, 3 mm, while the other parameters are kept the same as the base line.

The results of liquid fraction and temperature distribution obtained from different thickness scenarios are shown in Figure 3.13. On the left side, the 3 mm thick ring scenario has the largest ice generated area at 1800 seconds. On the second row of liquid fraction, water in the middle of rectangular space formed into ice completely with the 1 mm, 2 mm and 3 mm rings at 3600 seconds. On the third row of liquid fraction, water in all cases within the thin layer ring turned into ice at 7200 seconds, but ice formation at the center in the case without thin layer ring didn't achieve completely. Moreover, the temperature distribution on the right side shows similar results. The

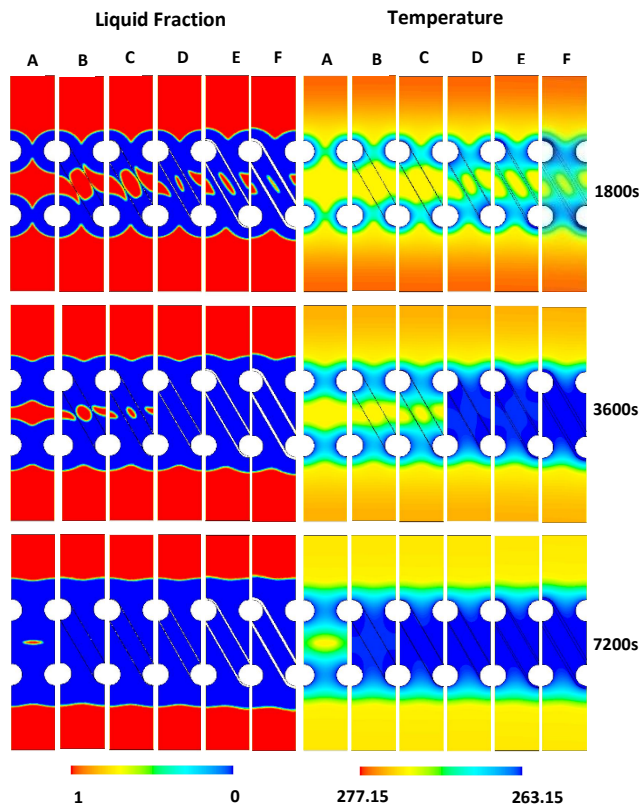


Figure 3. 13 Liquid fraction (left) Temperature (right)

A (without ring), B (0.25 mm), C (0.5 mm)

D (1 mm), E (2 mm), F (3 mm)

temperature near the thin layer ring is lower in the space and relatively much lower near the thicker ring. However, it is also found that the 2 mm thin layer ring can approximately reduce the temperature to the same degree as the 1 mm thin layer ring case at 3600 seconds, since the thicker ring has the higher resistance in the conductive heat transfer. Also, the center temperature in the 0.25mm and 0.5 mm thin layer is not as high as the other two thickness cases due to the decreased thickness.

The temperature at the center point, shown in Figure 3.14, took nearly 800 seconds to reach the lower limit of the phase transition temperature for the five cases with thin layer ring. However, it took 2000 seconds for the case without the ring. After that, the temperature at the center point in 6 different cases remains constant during the phase transition of water from liquid to solid. At the start of the phase transition, heat transfer was primarily by convection within the water region and by conduction after water turns into ice. This is because during ice formation, the rate at which energy was absorbed from the refrigeration cylinder balanced the rate at which energy was transferred to the adjacent phase changing material, as a result of the temperature gradient in the

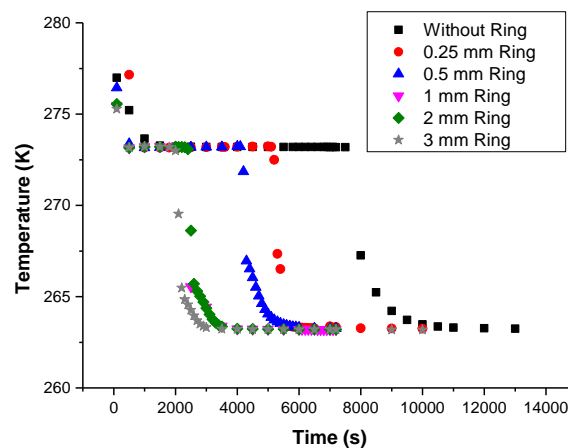


Figure 3. 14 Temperature variation in the middle vs. time

rectangular region. The latent heat transfer time is between 800 seconds to 5200 seconds in the 0.25mm aluminium case, between 800 seconds to 4100 seconds in the 0.5 mm case, between 800 seconds to 2200 seconds in the 1mm case, between 800 seconds to 2400 seconds in 2 mm case, between 800 seconds to 1900 seconds in the 3 mm case and between 2000 to 7500 seconds in the none wing case. An interesting phenomenon was observed, the thinnest case with 0.25 mm ring took longer than other four thicknesses from 800 seconds to 5200 seconds during the latent heat transfer process, since the ring is too thin to absorb heat from the water and to transfer the heat to refrigeration cylinder through conduction. A rapid drop of the phase transition temperature occurred from 7500 seconds in the case without the ring at the start of the sensible heat transfer process and continued changing until the temperature was close to the refrigeration temperature of 263.15K at 130000 seconds. This similar process also occurred from 5200 seconds to 6300 seconds in the 0.25 mm case, from 4100 seconds to 6500 seconds in the 0.5 mm case, from 2200 seconds to 4500 seconds in the 1 mm case, from 2400 seconds to 3500 seconds in the 2 mm case, from 1900 to 3000 seconds in the 3 mm case.

3.4.4 Effect of arrangement

Changing in the arrangement of thin layer ring will result in variation of heat transfer area, which would change heat transfer rate. Therefore, three different arrangements are analyzed in this study to investigate the effect of arrangement: staggered, 1 parallel, and 2 parallel scenarios, while the other parameters, such as material and thickness are kept the same as the base line. The geometry of these three arrangements of the thin layer ring is shown in Figure 3.15. For the staggered arrangement, the thin layer ring is deployed across the center area. For the 1 and 2 parallel arrangement, the thin layer ring is attached to two neighbouring cooled cylinders. The results of liquid fraction and temperature distribution are presented in Figure 19. On the left side, it can be

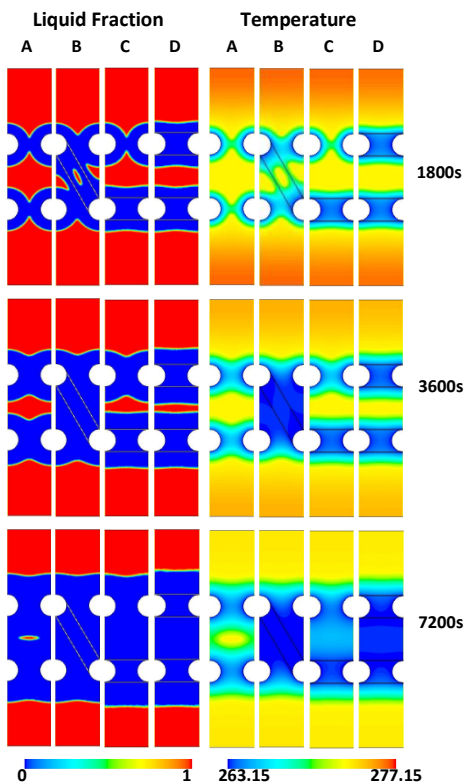


Figure 3. 15 Liquid fraction (left) Temperature (right): A (without ring), B (staggered), C (1 parallel), D (2 parallel)

seen that the ice generated area from the staggered case is obviously more than that generated from the parallel cases at 1800 seconds. At 3600 seconds, water in the middle space is completely frozen for the staggered case, while it's not shown in the other cases. However, such areas are nearly the same at 7200 seconds when thin layer ring applied. Results on the right side shows that temperature between two parts of the thin layer ring in the parallel is colder compared to the area not surrounded by thin layer ring throughout the whole ice formation process. The staggered case shows the best heat transfer performance among these three scenarios.

The temperature at the center point, shown in Figure 3.16 took nearly 800 seconds to reach the lower limit of the phase transition temperature for the staggered case, the 1 parallel case, and the 2 parallel case. However, it took 2000 seconds for the case without the ring. After that, the temperature at the center point in 4 different cases remains constant during the phase transition of water from liquid to solid. The latent heat transfer region is between 800 seconds to 2200 seconds in the staggered case, between 800 seconds to 5500 seconds in 1 parallel case, between 800 seconds

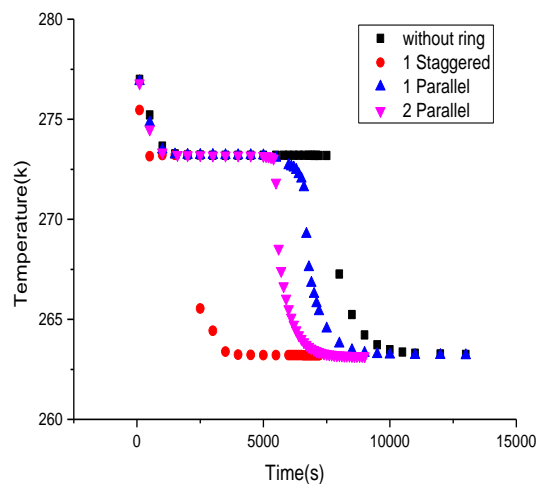


Figure 3. 16 Temperature variation in the middle vs. time

to 5000 seconds in 2 parallel case and between 2000 to 7500 seconds in the none wing case. The result of this process is well predicted, since 2 parallel case has increased heat transfer area. The latent heat transfer rate is greater than 1 parallel case. A rapid drop of the phase transition temperature occurred from 7500 seconds in the case without the ring at the start of the sensible heat transfer process and continued changing until temperature is close to the refrigeration temperature of 263.15K at 130000 seconds. This similar process also occurred from 2200 to 4500 seconds in the staggered case, from 5500 seconds to 9000 seconds in the 1 parallel case, from 5000 seconds to 8000 seconds in the 2 parallel case.

3.5 Factorial effect analysis of thin layer ring by Taguchi method

Using the thin layer ring in the ice storage tank has been proved effective from the previous computational results, since the time of the ice formation can be shortened and the area ratio can be increased. In other words, the overall efficiency of ice thermal storage system can be improved. However, there is a large arrangement space as well as different placement strategies which need to be investigated for the utilization of a thin layer ring for the improvement of an ice thermal storage system. This is to say, many unknown parameters and different arrangements should be explored and determined on their variations in details. For this reason, material, thickness, and different placements were investigated initially for the thin layer ring structure. The baseline shown in Table 3.3 with three constant parameters was used to compare with different cases using different parameters and values.

3.5.1 Selection of characteristics

In general, heat transfer enhancement in ITS system results in increasing the ice generated area during the same time period and shortening ice formation time. Therefore, a new parameter is defined to evaluate increased ice area for the Taguchi analysis. Usually, there are three categories of the performance characteristic in the analysis, which are the smaller-the-better, the larger-the-better and the nominal-the-better. In this study, IA factor introduced in this study stands for increased ice formation area during the same period. IA factor is also a number of larger-the-better characteristics showing the percentage of the increased ice generated area compared to the case without thin layer ring, and is defined as follows.

$$IA = \frac{A_{TLR@SamePeriod} - A_{bare@SamePeriod}}{A_{bare@SamePeriod}} \times 100 \quad (3.8)$$

Where, $A_{TLR@SamePeriod}$ is area generated by thin layer ring during the same period as bare case, and $A_{bare@SamePeriod}$ is area generated without thin layer ring during the same period as thin layer ring case.

3.5.2 Factor and levels

In the Taguchi analysis, the control factors and their levels are firstly defined. The significance of different parameters, such as material, thickness, arrangement investigated will be addressed. Base on the above study on the effectiveness of three parameters, the levels of each factor in this study are shown in Table 3.5 in order to perform the comparison study of each parameter.

Table 3. 5 Levels of each factor

Code	Factors(unit)	Level 1	Level 2	Level 3
A	Material	Aluminium	Stainless Steel	Copper
B	Thickness (mm)	0.5	1.0	2.0
C	Arrangement	Staggered	One parallel	Two Parallel

3.5.3 Orthogonal array

According to the numerical database analysed above, an orthogonal array of L₉ (3×3) is designed for study as shown below in Table 3.6.

3.5.4 SN analysis

In the quality engineering and experimental design, the SN ratio (signal to noise ratio) was firstly introduced by Taguchi and has also been widely used. The SN ratio is calculated from the following equation. After the analysis of the SN ratio, the main effective factors could be determined, and the interaction of each parameter could be more clearly understood. Considering the characteristics of the subject, the larger the better scenario is taken into consideration in the study.

$$SN(= \eta) = -10 \log \left[\frac{1}{IA^2} \right] \quad (3.9)$$

Table 3. 6 The orthogonal array of L9

Number of test	A	B	C
Test 1	1	1	1
Test 2	1	2	2
Test 3	1	3	3
Test 4	2	1	2
Test 5	2	2	3
Test 6	2	3	1
Test 7	3	1	3
Test 8	3	2	1
Test 9	3	3	2

Table 3. 7 SN ratio on each case

Number of test	A	B	C	IA	SN Ratio(η)
Test 1	1	1	1	21.79	26.7668
Test 2	1	2	2	11.4942	21.2096
Test 3	1	3	3	13.4051	22.5454
Test 4	2	1	2	3.3247	10.4350
Test 5	2	2	3	8.9204	19.0077
Test 6	2	3	1	7.8325	17.8781
Test 7	3	1	3	23.4918	27.4183

Test 8	3	2	1	27.9337	28.9226
Test 9	3	3	2	14.6284	23.3040

3.5.5 Taguchi Analysis

The SN ratio calculated from the nine numerical simulations is presented above in Table 3.7. With the SN ratio obtained, the contribution ratio of every factor can be calculated and shown in the Table 3.8. In the Table 3.8, the Δ is the difference between the maximum and minimum of the SN ratio for each factor. After adding up all the Δ of each factor, the total Δ is equal to 18.78. After that, to evaluate the influence of each factor on the percentage of increased ice area (IA), the contribution ratio is then introduced. The contribution ratio equals to the value of the Δ of each factor divided by the total Δ of all factors. Therefore, the main effective factors could be determined. By the calculation, the contribution ratio of each factor can be obtained as follows: 57.35% for material, 9.58% for thickness, 33.07% for arrangement. It can be obviously seen in Figure 3.17. That means material has the most impact on the percentage of increased ice area when using thin layer ring structure, while other factors have relatively less influence on ice generated area. Based on these results, in the design process, material should be given more considerations. Next is the arrangement of thin layer ring. Finally, thickness is the third factor to be considered.

Table 3. 8 Factorial effect and contribution ratio

	Level	A	B	C
SN ratio	1	23.51	21.54	24.52
	2	15.77	23.05	18.32
	3	26.55	21.24	22.99
Δ (Max-Min)	18.78	10.77	1.80	6.21
Contribution ratio (%)	100%	57.35%	9.58%	33.07%
Rank		1	3	2

The above analyses on the contribution ratio are limited to evaluating the significance of these three factors only. To determine the optimal design, the SN ratio of each factor should be taken into further consideration. From the Figure 3.18, the largest SN ratio among the 3 levels stands for the best performance when using the Taguchi method for the experimental design. Fig.3.18 shows the results below. For the factor A (material), level 3 (Copper) is the best. Level 2 (1mm) is the best for the factor B (thickness). For the factor C (arrangement), level 1 (staggered) is the best. However, the factor B has insignificant effect on ice generation area. From the results presented above, material, thickness, arrangement have the optimal condition when set as copper, 1mm, staggered, respectively.

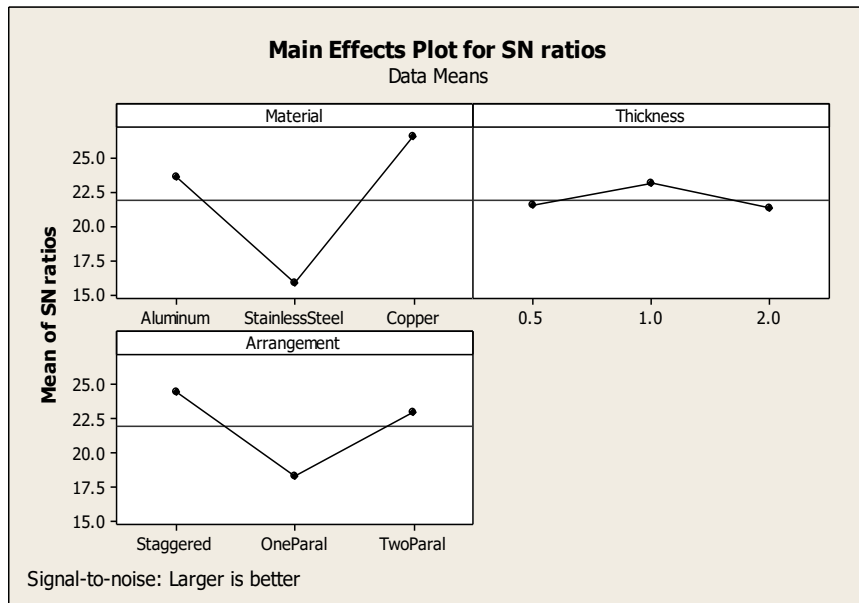


Figure 3. 18 SN ratio on each factor

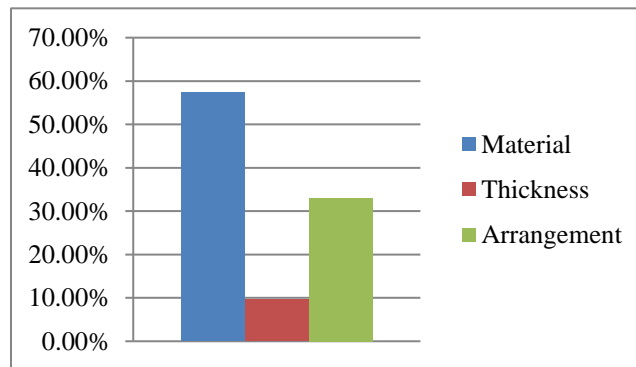


Figure 3. 17 Contribution ratio on each factor

3.5.6 Determination of the optimal condition

After running Taguchi method, the optimal condition can be obtained by a combination of levels presenting the largest SN ratio in each control factor as shown in Table 3.6. As a result, two optimal conditions are selected in this study as shown in Table 3.7. However, in reality, only one optimal condition can be obtained using the present method, but the second optimal condition is also taken

into consideration for the confirmation test. Therefore, one original optimal condition is determined based on the Taguchi analysis method, and the second optimal condition is selected to eliminate the error of analysis and find the best condition. These two optimal conditions are A3B2C1 and A1B1C3, respectively.

3.5.8 Reproducibility by confirmation test

The two test samples combined with the three factors were designed and selected to be the optimal conditions as described above for the confirmation test. These two conditions and factors are shown in Table 3.9. Two methods were adopted into the confirmation test.

Table 3. 9 Optimal conditions from factorial effect analysis

Optimal Condition	Condition 1	Condition 2
Material	Copper	Aluminium
Thickness	1 mm	0.5 mm
Arrangement	Staggered	2 Parallel

The first method was to compare the presumed SN ratio for the optimal condition and the SN ratio of confirmation test results for the optimal samples. η_{pre} is the presumed SN ratio calculated based on the following equation.

$$\eta_{pre} = \eta_{A3} + \eta_{B2} + \eta_{C1} - 2 \times \bar{\eta} \quad (3.10)$$

$$\eta_{pre} = 26.55 + 23.05 + 24.52 - 2 \times 21.94 = 30.24 \quad (3.11)$$

In the above equation, values were selected as the largest SN ratio for each factor and taken from Table 3.7. $\bar{\eta}$ is taken as the average value of nine S/N ratio in Table 3.7. Therefore, the presumed η_{pre} was 30.24. However, the SN ratio of the optimal Condition 1 was directly obtained from Table 3.7, which is 28.9226. Since the presumed η_{pre} is greater than that of Condition 1 and they are very close to each other, that is to say the existence of reproducibility in this condition is confirmed.

Hence, the second method is to confirm the reproducibility by comparing IA factor of Condition 1 and Condition 2. From the previous analysis, IA factor of Condition 1 is directly obtained from Table 3.7, which is 27.9337. The result from the simulation of Condition 2 showed IA factor of Condition 2 is 11.6. The IA factor of the optimal Condition 2 is lower than that of the optimal Condition 1 and there is no interaction between three parameters. Therefore, it is demonstrated that the optimal Condition 1 performs better than the optimal Condition 2 and all others. That is to say it is the ultimate combination of thin layer ring's three parameters.

In Figure 3.19, it shows the time-wise temperature change for the condition 1, condition 2 and the baseline. For the condition 1, the temperature drops before 2000 seconds and then reaches the lower limit of the phase transition point which is latent heat transfer starting point. However, the condition 2 takes longer than condition 1. Moreover, the baseline forms ice longest among all combinations including the condition 1 and condition 2. Figure 3.20 shows the liquid fraction and temperature distribution of the analyzed domain for the condition 1 and condition at 3600 seconds. It is obvious that ice is generated more by condition 1 than condition 2 in the figure showing liquid fraction, in which 1 indicates the liquid state and 0 indicates the solid state. In the figure of

temperature distribution, the area of condition 1 shows much colder than condition 2, since it has better heat transfer combination of three parameters of thin layer ring.

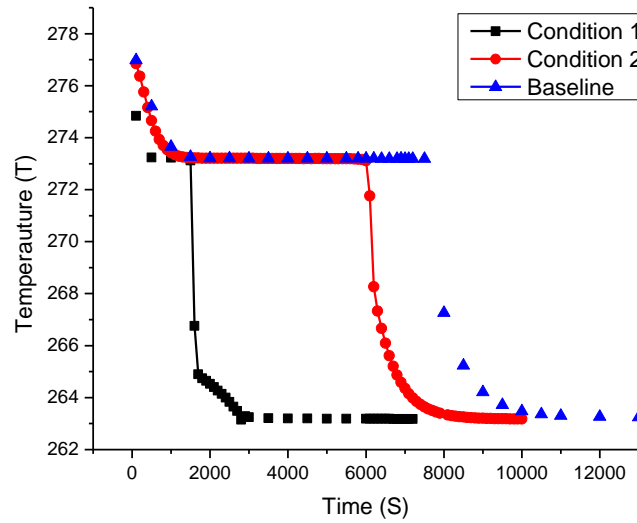


Figure 3. 19 Time-wise temperature during ice formation

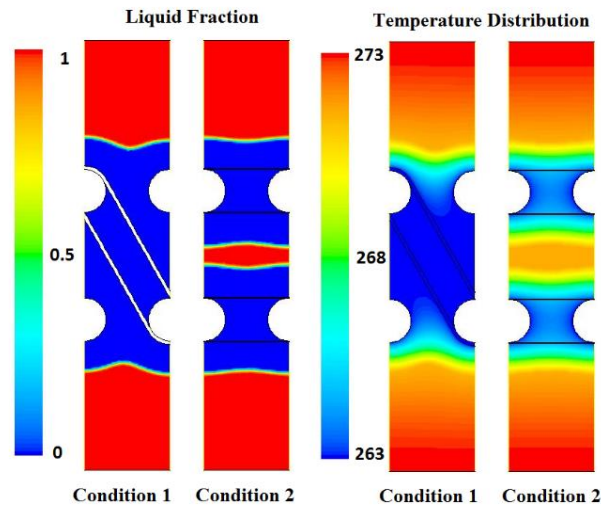


Figure 3. 20 Liquid fraction and temperature distribution of condition 1 and condition 2

From the preliminary exam focused on thermal performance enhancement using thin layer ring in ITS system, the impact of the different parameters of thin layer ring on ice formation has been evaluated and investigated by the numerical method. Moreover, the optimal parameters and conditions have been determined by the Taguchi method. The main results of this study will be presented in the Chapter 5.

CHAPTER 4 NUMERICAL STUDY OF VORTEX STRUCTURE IN BETTERY ENERGY STORAGE SYSTEM

4.1 Introduction

This study is focused on one battery cell with an air flow channel for the numerical simulations. Among all types of battery cell such as coin cell and cylinder cell, pouch cell as a single unit in the LIB application is a preferred power source for electric power usage (Karimi and Dehghan 2014) and has 84% share of the market (De-Leon 2010). Therefore, numerical simulations were carried out to investigate the thermal behavior and performance of proposed new structure, vortex generator applied on the surface of a pouch cell for the cooling enhancement. Two types of VGs are included in the study, which are rectangular rib and delta winglet. In terms of battery cell components in the study, a LiMn_2O_4 cathode battery is selected, since it is very popular and ideal material as a high-capacity Li-ion battery cathode with the benefits of low toxicity and low cost. Since other research has conducted an experiment with this type of battery (Seong Kim, Yi et al. 2011), the numerical model can be validated with their experiment results. The results from this study would provide a better understand of using VG for LIB pouch cell cooling and become a guideline for the further experimental research.

4.2 Numerical model description

4.2.1. Physical model

Battery domain:

A LiMn₂O₄ cathode, a graphite anode and a plasticized electrolyte are comprised of a 14.6 Ah lithium-ion pouch cell for the numerical study. A cell consisting of two parallel plate electrodes of the battery shown in Fig. 4.1 with full cell dimensions. Cell itself consists of the same repeating units of positive and negative electrode plates, polymer electrolytes and separators. In Figure 4.1, the current collecting tabs are the current collectors extending outside the rectangular electrodes and they do not contain the electrode (active) material. Since the distance between the electrodes was so small in the study, the current flow between the electrodes is assumed to be perpendicular to the electrodes. The modelling procedure used to calculate the potential and current density distribution on the electrodes was similar to that used by Kwon et al.

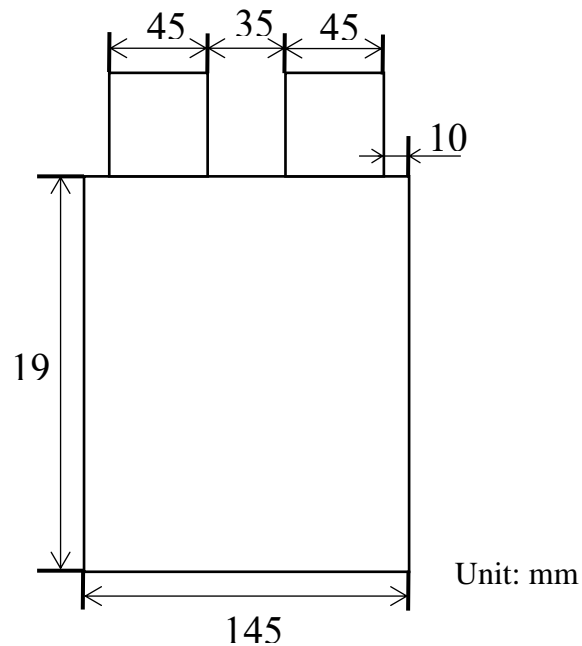


Figure 4. 1 Geometry of Pouch Cell

From the continuity of the current on the electrodes, the following equations can be derived:

$$\nabla \cdot \vec{i}_p - J = 0 \text{ in } \Omega_p \quad (4.1)$$

$$\nabla \cdot \vec{i}_n - J = 0 \text{ in } \Omega_n \quad (4.2)$$

$$\vec{i}_p = -\frac{1}{r_p} \nabla V_p \text{ in } \Omega_p \quad (4.3)$$

$$\vec{i}_n = -\frac{1}{r_n} \nabla V_n \text{ in } \Omega_n \quad (4.4)$$

The following polarization is expressed in the mathematic model.

$$J = Y(V_p - V_n - U) \quad (4.5)$$

U and Y are depicted as functions of the depth of discharge (DOD) below.

$$U = a_0 + a_1(DOD) + a_2(DOD)^2 + a_3(DOD)^3 \quad (4.6)$$

$$Y = a_4 + a_5(DOD) + a_6(DOD)^2 + a_7(DOD)^3 + a_8(DOD)^4 + a_9(DOD)^9 \quad (4.7)$$

Where, a_0 - a_9 are the constant values that adjust the modelling results to the best experimental data at an environmental temperature of 25°C. The values of them in the calculation of potential and

current density distribution on the electrodes are shown in Table 4.1. Other thermal properties are shown in Table 4.2.

Table 4. 1 Property of the constant values

Property	Spec.	Property	Spec.
a_0 (V)	4.12	A_5 (A/m ²)	-892.8001
a_1 (V)	-0.804	A_6 (A/m ²)	5250.46
a_2 (V)	1.075	A_7 (A/m ²)	-13623.09
a_3 (V)	-1.177	A_8 (A/m ²)	15853.17
a_4 (A/m ²)	116.859	A_9 (A/m ²)	-6757.8539

Table 4. 2 Parameters used for the thermal modelling

Component	Density (g/cm ³)	Heat capacity (J/g.K)	Thermal conductivity (W/cm.K)
Current collect of positive electrode	2.7	0.9	2.38
Electrode material of positive electrode	1.5	0.7	0.05
Current collector of negative electrode	8.96	0.385	3.98
Electrode material of negative electrode	2	0.7	0.05
Separator	1.2	0.7	0.01
Pouch	1.15	1.9	0.16*10 ⁻²

The following modified the expressions of U and Y are adopted to simulate the discharging behaviors at the different environmental temperatures other than 25°C.

$$Y = Y_0 \exp \left\{ -C_1 \left(\frac{1}{T_{abs}} - \frac{1}{T_{abs,0}} \right) \right\} \quad (4.8)$$

$$U = U_0 - C_2 (T_{abs} - T_{abs,0}) \quad (4.9)$$

$$DOD = \frac{\int_0^t J dt}{Q_T} \quad (4.10)$$

$$\rho C_p \frac{\partial T}{\partial t} = \frac{\partial}{\partial x} \left(k_x \frac{\partial T}{\partial x} \right) + \frac{\partial}{\partial y} \left(k_y \frac{\partial T}{\partial y} \right) + q - q_{conv} \quad (4.11)$$

$$q = aJ \left[E_{oc} - E - T \frac{dE_{oc}}{dT} \right] + a_p r_p i_p^2 + a_n r_n i_n^2 \quad (4.12)$$

$$q_{conv} = \frac{2h}{d} (T - T_{air}) \quad (4.13)$$

4.2.2 Flow domain

The governing equations which describe the conservation of mass, momentum, and energy in the computational fluid domain can be expressed below:

Continuity equation:

$$\frac{\partial}{\partial x_i}(\rho u_i) = 0 \quad (4.14)$$

Momentum equation:

$$\frac{\partial}{\partial x_i}(\rho u_i u_k) = \frac{\partial}{\partial x_i} \left(\mu \frac{\partial u_k}{\partial x_i} \right) - \frac{\partial p}{\partial x_k} \quad (4.15)$$

Energy equations:

$$\frac{\partial}{\partial x_i}(\rho u_i T) = \frac{\partial}{\partial x_i} \left(\frac{k}{c_p} \frac{\partial T}{\partial x_i} \right) \quad (4.16)$$

The boundary conditions for all surfaces are described as follows:

Velocity is 4m/s and Re is kept in the range of laminar flow.

(1) In the upstream extended

i. At the inlet boundary

$$u = u_{in} = const,$$

$$v = w = 0, T = T_{in} = const,$$

At the top and bottom boundaries

(2) Downstream of the exit, the streamwise gradients are zero

i. $\frac{\partial u}{\partial y} = \frac{\partial v}{\partial x} = \frac{\partial w}{\partial x} = \frac{\partial T}{\partial x} = 0$

(3) Upper and lower boundary condition:

i. On the wall, $u = v = w = 0$

(4) At side walls ($x=$; $x=$), symmetry condition:

$$\frac{\partial u}{\partial x} = \frac{\partial w}{\partial x} = 0, v = 0 \text{ (symmetry) and } \frac{\partial p}{\partial x} = 0$$

$$\frac{\partial T}{\partial x} = 0$$

4.3 Numerical method and parameter definitions

The governing equations along with the boundary conditions presented above were solved by the commercial finite-volume based solver, Fluent. In the flow domain, the governing equations for momentum and energy in conservative form were discretized with finite-volume formulation using an implicit order of accurate upwind differencing scheme. The scheme has second-order accuracy in space and first order accuracy in time and potential. A pressure-velocity based on the SIMPLE algorithm is adopted with least squares cell based gradient.

Parameter definitions:

The performance parameters depend on the channel geometry and flow conditions. For this type of vortex generator arrangements, the flow characteristics and heat transfer performance data will be presented. At the same time, results for a cooling channel on a pouch cell without VG will also be presented as a comparison to the channel embedded with different configurations of vortex generators (rectangular rib and delta winglet).

$$Re = \frac{\rho u_m D_h}{\mu} \quad (4.17)$$

$$Nu = \frac{h D_h}{k} \quad (4.18)$$

$$h = \frac{q}{\Delta T} \quad (4.19)$$

where u_m is the mean air velocity entering the channel.

The temperature difference is defined as: $\Delta T = T_w - T_m$

Therefore, the local heat transfer coefficient h_x is expressed as:

$$h_x = \frac{q_x}{T_w - T_m} \quad (4.20)$$

Where q_x is the average heat flux at a specific cross section of the channel, and T_m is the bulk mean temperature at that cross-section. T_w is the wall temperature.

4.4 Solution method and model validation

In order to validate the solution independency of the grid number, five different grid number were tested for the inlet velocity = 4m/s, therefore the flow is maintained as laminar in the flow domain, which are 1,187,003. Nusselt numbers (in fully-developed region) with different grid numbers are presented in Figure 4.2. It can be seen that the Nusselt number nearly remains a constant value (difference less than 5%) when the grid number is higher than 1,000,000. To ensure the accuracy of computation, the grid number was set to be above 1,000,000.

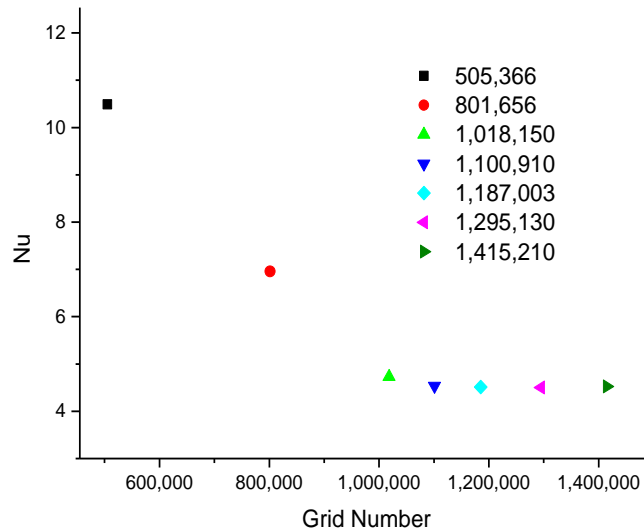


Figure 4. 2 Validation of grid number

Apart from the investigations on the grid independency, the characteristics of pouch cell are compared with the available experimental results. The reliability of the numerical method has also been validated with the experimental results from the same geometrical and material pouch cell presented in Kim's research (Seong Kim, Yi et al. 2011). The inlet air velocity is 4 m/s and the corresponding Re number in investigated channel is less than 2,000. The predicted results are compared with the experimental results from Kim's work (Seong Kim, Yi et al. 2011). The

discharge curves and maximum cell temperatures between the numerical study and experimental

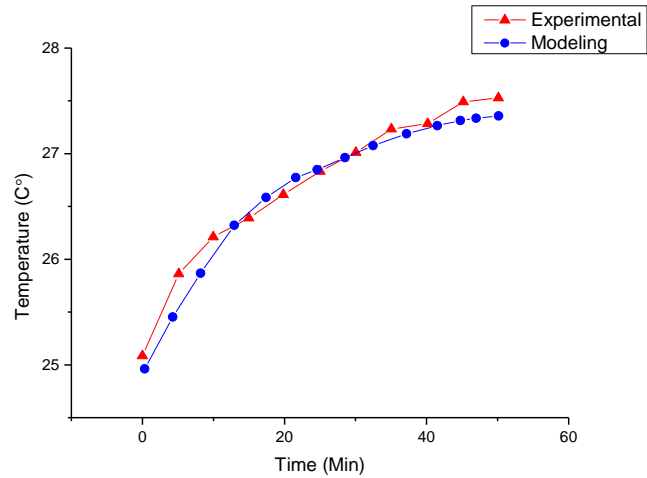


Figure 4. 4 Temperature curve between experimental and numerical studies

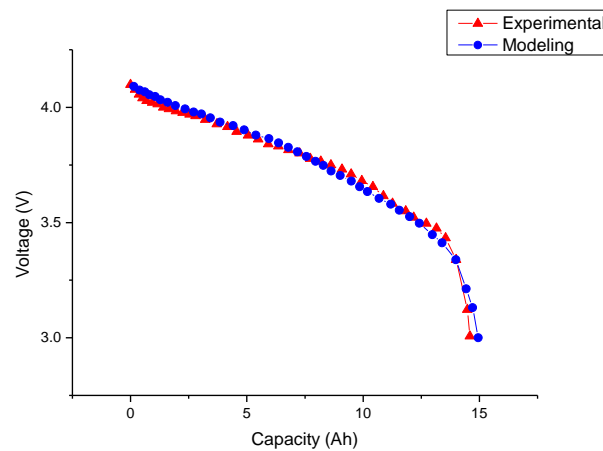


Figure 4. 3 Potential curve between experimental and numerical studies

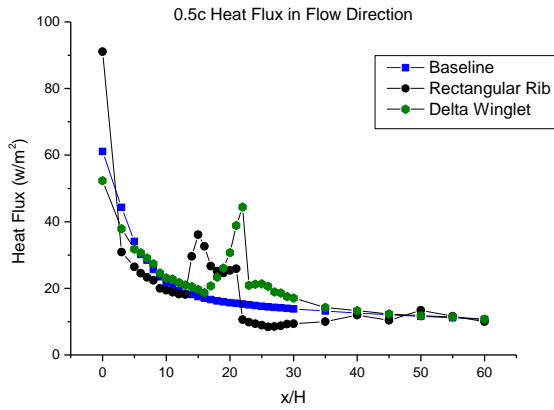
study at 1C discharging rate are shown in Figure 4.3 and Figure 4.4, respectively. The discrepancy between the numerical and experimental results is less than 5%. The good agreement between the numerical and experimental results indicates that the present numerical pouch cell with convection cooling is reliable to predict heat transfer characteristics of cell and flow domain.

4.5 Results and discussion

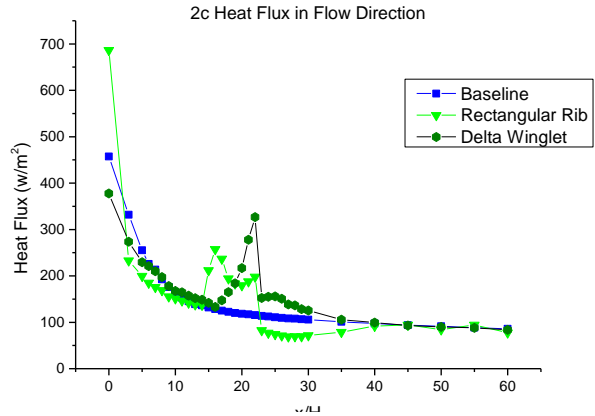
4.5.1 Heat transfer

Time-dependent transient simulations in a three-dimensional flow channel with a pouch cell at the bottom were performed for three scenarios: baseline without VG, rectangular VG and winglet VG. No initial assumption was made regarding the development of flow and thermal conditions. After simulation, the air flow reached a statistically steady state of 50H (H=2mm). The heat transfer performance results for both rectangular rib and winglet were compared to the baseline results. Air flow computations were performed at air-side flow conditions corresponding to $Re=1,044$. The simulation parameters are summarized as follows:

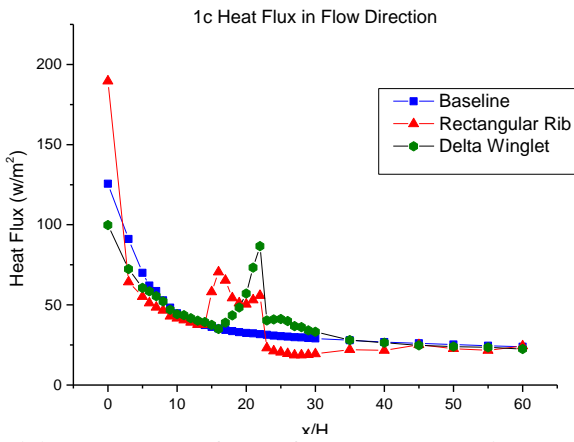
Air inlet velocity: 4 m/s; Air inlet temperature: 393.15 K; Time step size: 30 second



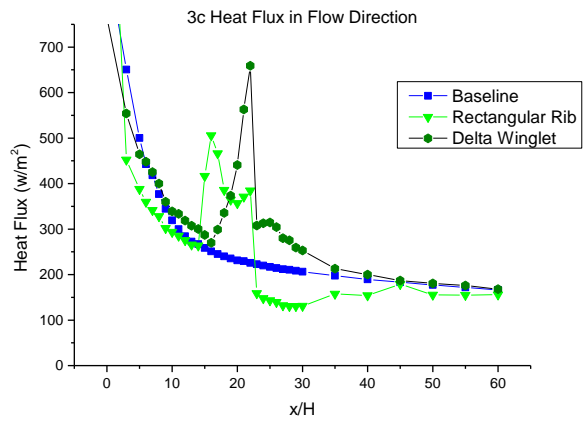
(a) Local heat flux of rectangular and delta winglet at 0.5c



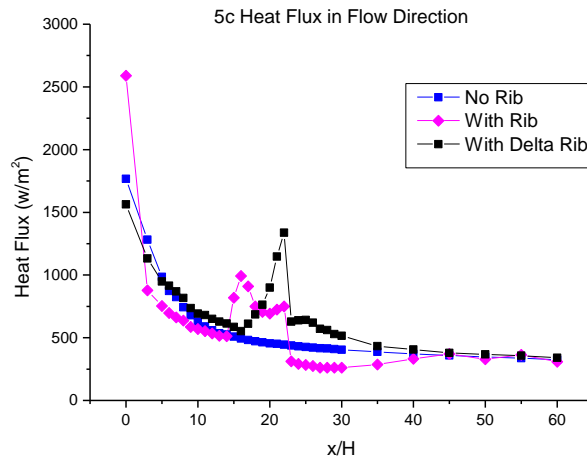
(c) Local heat flux of rectangular rib and delta winglet at 2c



(b) Local heat flux of rectangular rib and delta winglet at 1c



(d) Local heat flux of rectangular rib and delta winglet at 3c



(e) Local heat flux of rectangular rib and delta winglet at 5c

Figure 4. 5 Local heat flux of rectangular rib and delta winglet at 0.5c, 1c, 2c, 3c, 5c

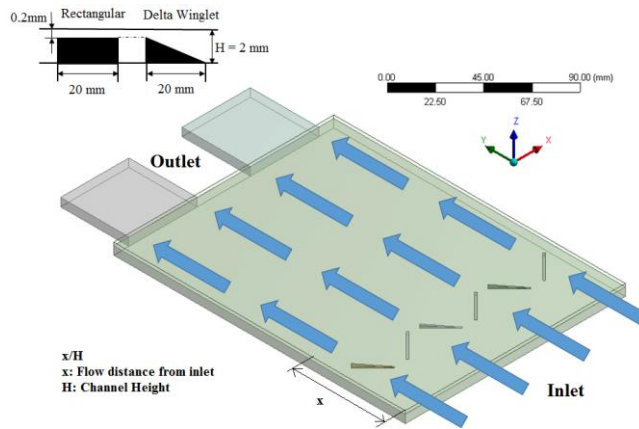


Figure 4. 6 Illustration of flow domain

The local heat flux curves for the baseline, rectangular rib and winglet are compared in Figure 4.5 at 0.5c, 1c, 2c, 3c and 5c discharging rates. The baseline at all discharging rates has a very smooth drop in the flow direction, corresponding to the longitudinal direction of the pouch cell. Figure 4.6. shows the placement of two types of vortex generator and their dimensions. The thickness of each VG is 1mm. From the results of heat flux, Figure 4.5(a) shows the heat flux curve along the flow direction at a rate of 0.5c. The heat flux curve for the rectangular rib scenario first peaks at $x/H=15$. The increase of local heat flux is due to the rectangular geometry of vortex rib when it is deployed at $x/H=13$ from air flow inlet. Since rectangular rib creates more heat transfer surface on the pouch cell, it is obvious that local heat flux should be higher from the leading edge of rib to the end of rib. However, it slightly drops after the first peak, since the special rectangular geometry doesn't change significantly along the flow direction. However, the heat flux curve for the rectangular rib scenario second peaks nearly at the end of rib. The second peak is due to the geometry change from rectangular rib to the plain channel. The side surface of rectangular rib increases heat flux. After the second peak, local heat flux has a drastic drop immediately after rectangular rib. Compared to the baseline, local heat flux in the rectangular rib scenario is even lower. Even though

rectangular rib can increase local heat flux when it is mounted from $x/H=13$ to $x/H=22$, the benefit to increased heat flux can be also offset after the deployment. However, the local heat flux curve with winglet vortex generator is different from the rectangular rib scenario. Figure 4.5(a) also shows that there is only one peak on the delta winglet curve along the flow direction. From the leading edge of winglet, local heat flux starts to increase significantly at $x/H=15$. Due to the delta shape of winglet geometry, heat flux gradually increases along the edge of winglet, since the heat transfer surface of the pouch cell is increased by the delta winglet VG, which is similar to the rectangular rib scenario. The local heat flux increases until it peaks at $x/H=23$, then a sudden drop occurs after the delta winglet VG. However, the local heat flux curve in delta winglet scenario can remain above the curve in the baseline scenario, which means thermal effort on local heat flux in the delta winglet scenario still exists after the air flow passes the delta winglet VG. Heat flux can be affected until air flow reaches $x/H=35$. Three curves between the baseline, rectangular rib and delta winglet are nearly identical to each other after $35H$ until air reaches the end of flow channel. As discussed above, local heat flux can be both increased by rectangular rib and delta winglet before $x/H=23$, which means heat transfer performance in two scenarios can be both enhanced by two types of vortex generator when air flow passes through them. However, both vortex generators have advantage and disadvantage after $x/H=23$. Compared to the baseline scenario, local heat flux is higher in the delta winglet scenario, but lower in the rectangular rib scenario. That is to say delta winglet can increase local heat flux, while rectangular rib decreases it after $x/H=23$. Since rectangular rib was mounted on the pouch cell, some portions of air flow could be blocked and air flow rate could be reduced completely behind the rib. However, it is partially blocked with delta winglet VG, air can still move across each delta winglet VG. Therefore, some vortices generated

by delta winglet VG can still affect local heat flux over a long distance to $x/H=35$. After it, three different curves are also overlapped and nearly the same. Flow structure of three scenarios will be presented later.

Compared with different heat flux curves at different discharging rates, the highest heat flux is always at air inlet. It drops in the flow direction, but has an increase near both types of vortex generators. Eventually, it drops to a static state and remains nearly constant after $x/H=45$, which is 90mm from air inlet. It can be seen that static heat flux at the end of channel is nearly 18w/m^2 at discharging rate of $0.5c$, 25 w/m^2 at rate of $1c$, 100 w/m^2 at rate of $2c$, 200 w/m^2 at rate of $3c$ and 450 w/m^2 at rate of $5c$, respectively. As the results shown in Figure 4.5 (a, b, c, d and e), it implicates that both vortex rib can enhance conductive and convective heat transfer from the inside of pouch cell to the outside of pouch cell due to increased heat transfer area and vortices generated by two types of VG on the cell surface.

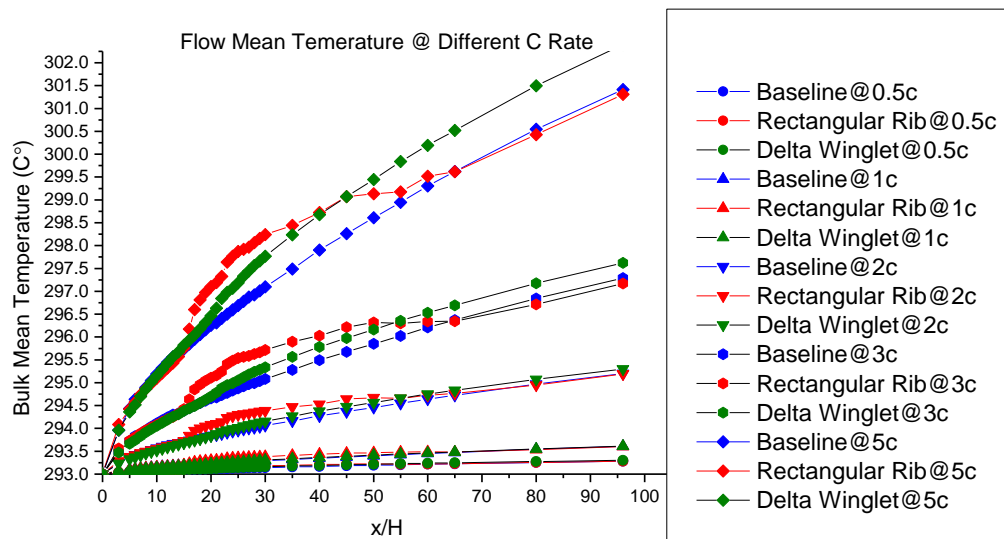


Figure 4. 7 Buck mean temperature of three scenarios at 5 different C rates

Figure 4.7 shows the mean temperature of air flow in the flow direction at 5 different discharging rates. From the temperature profiles, it can be clearly seen that the temperature of air rise along the flow direction for 3 different scenarios. Since the local heat flux mentioned above depends on the discharging rate, higher temperature of cell surface can be observed at higher discharging rate, which leads to higher temperature of air flow in the channel. Therefore, the baseline temperature difference between the channel entrance and $x/H=96$ (192mm) is nearly 8.25k, 4.5k, 2.25k, 0.5k and 0.25k for the discharging rate of 5C, 3C, 2C, 1C, 0.5C, respectively. That is to say battery cell at higher discharging rate generates more heat and should be cooled down more than the battery operating at lower discharging rate. In order to secure battery operation, temperature control is very critical at higher discharging rate. This study will later show some results related to maximum temperature drop after VG installed at higher discharging rate.

Although three different scenarios have similar trend of temperature increase in the air flow direction, temperature increases for a longer distance in delta winglet scenario than in rectangular rib scenario. Due to two different VG geometries, flow temperature increases rapidly in rectangular rib scenario after air flows over it, while it is not very obvious that air flow temperature increases significantly in delta winglet scenario before the leading edge. At discharging rate of 5c, temperature increases more by rectangular rib after air flows over VG. The similar phenomena can also be observed at other discharging rates, but air flow temperature at 5c is increased more obviously and significantly compared to other discharging rates. On the other hand, battery at 5C

is a good testing rate for such study. At discharging rate of 5c, temperature in the rectangular rib scenario decreases and then becomes lower than the temperature in delta winglet scenario after air moves across $x/H=42$ (84mm from the channel inlet). However, the temperature deviation between the baseline and delta winglet scenario remains nearly the same from $x/H=42$ to the end due to more vortices generated by delta winglet that can mix air flow completely in the cooling channel, so the temperature evenly increases in delta winglet scenario. At the other discharging rates, delta winglet has the similar results. From the perspective of mean air flow temperature, air temperature increases more in two VG scenarios than the baseline, but delta winglet has better thermal performance that can mix air evenly and completely, increase air temperature consistently and continuously until the end of cooling channel. This is because the rectangular blocks air flow completely and generates less vortices and the delta partially blocks air flow and generates more vortices that can mix hot and cold air completely along the flow direction. It is to say the vortices generated by vortex generator in the flow direction become an important factor effecting the cooling performance in the following flow channel after VG.

The results of local heat flux and mean air flow temperature show both types of vortex generator can enhance heat transfer performance by increasing cell surface heat transfer rate and temperature of cooling air in the channel, but both conductive and convective heat transfer were separately analyzed and the results show some benefits and penalties using two types of vortex generator. Figure 4.8 shows the local Nusselt number (Nu) along the flow direction for three different scenarios at 5 different discharging rates (0.5C, 1C, 2C, 3C and 5C). The local Nusselt number combining two effects of heat transfer between conduction and convection can evaluate the thermal performance of VG more comprehensively, since it is the ratio of convective heat transfer to conductive heat transfer. Compared to the non-cooling flow situation, it is revealed that using active air cooling can definitely and effectively enhance the cooling performance on the surface of battery cell. Moreover, using VG in the active cooling flow channel results in more enhancement on heat transfer. In Figure 4.8, the variation of Nusselt number along the flow direction are shown. It is clear that Nusselt number in the baseline scenario decreases smoothly. In the scenarios with rectangular rib and delta winglet VG, local Nusselt number with delta winglet has relatively

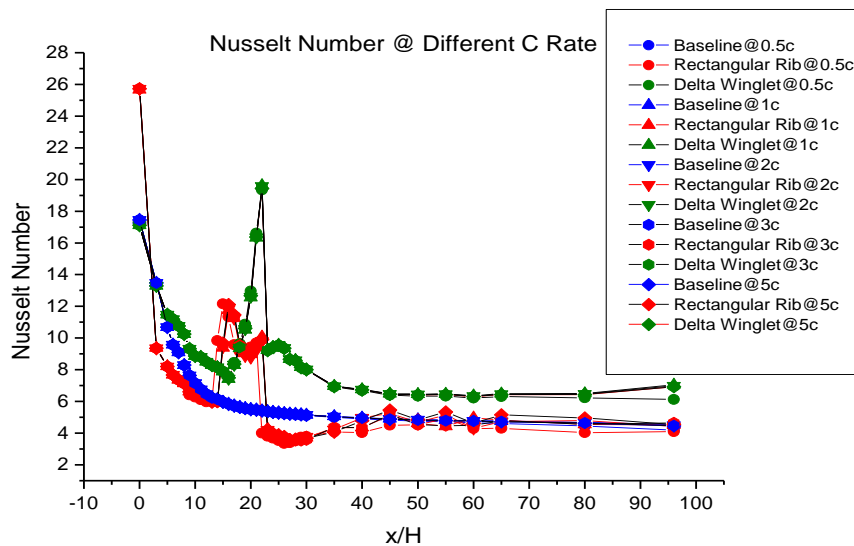


Figure 4. 8 Nusselt number of three scenarios at 5 different C rates

highest values in the region between $x/H=5$ and $x/H=14$, since most air is trapped in front of rectangular ribs due to its geometry. However, the result also reveals that local Nusselt number in the rectangular rib scenario has highest values in the region between $X/H=14$ and $x/H=18$, because rectangular ribs has a larger surface and transfers more heat to the surrounding air flow than delta winglet. After $x/H=18$, the Nu curves with delta winglet significantly increase until they reach the peak where the distance is at $x/H=22$ from the channel inlet. After $x/H=22$, Nusselt numbers of both rectangular rib and delta winglet decrease a lot within a short distance. Even though there is a drop of Nusselt number in the scenario with delta winglet, the local Nusselt numbers are still greater than the baseline. It is obviously seen that the baseline result is between rectangular rib and delta winglet in the region between $x/H=22$ and $x/H = 40$. Therefore, rectangular rib has relatively poor thermal performance among three in this region. It acts as a penalty with rectangular ribs between $x/H=22$ and $x/H=40$, but delta winglet is completely beneficial for the cell cooling. The local Nusselt number in the delta winglet scenario is always higher than other two scenarios after $x/H=18$. Because delta winglet generates more and larger vortices which facilitate the flow mixing, the thermal performance of it is better than rectangular rib. Since rectangular rib has a larger heat transfer surface, it only enhances heat transfer for a short distance when air flow crossing vortex generators and it has relatively lower Nusselt number which translates to poor heat transfer performance for a certain distance after rectangular rib. After $x/H=40$, Nusselt numbers of baseline and rectangular rib are very close to each other, since the effect of air flow blockage disappears after a certain distance where vortices newly generated by rectangular rib begin to enhance overall heat transfer again until air exits the channel. It can be concluded that the heat transfer

enhancement in both types of VG scenarios achieves in the region where the VGs are mounted, but only delta winglet can enhance it for a long distance in the downstream flow direction.

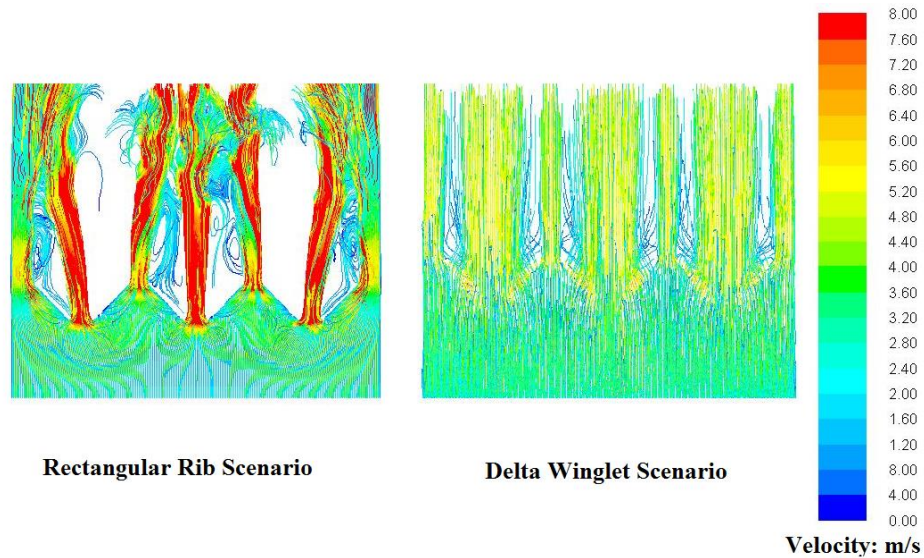


Figure 4. 9(a) Flow structure of rectangular ribs (b) Flow structure of delta winglet

4.5.2 Flow structure

Since the thermal behaviour of two types of VGs has been discussed previously. Meanwhile, it is also important to analyze the effect of VG on air flow structure. Therefore, Figure 4.9 shows the comparison of flow structure between rectangular rib scenario and delta winglet scenario from the top view of cooling channel. Figure 4.9 shows flow structure on the pouch cell surface in the rectangular rib scenario. The path lines before rectangular ribs are nearly uniform and velocity doesn't increase a lot. However, when air flow is crossing the rectangular ribs, the velocity of flow increases a lot and vortices are also being generated after rectangular ribs. Pressure drop also happens after rectangular ribs. There is nearly no path line behind each rib, so the velocity is low and pressure is relatively high. That is to say, there is less vortices generated behind rectangular

ribs that are benefit for the air mixing. Without enough vortices, air mixing between cold and hot air becomes incomplete, so it is the reason why heat transfer cannot be continuously enhanced after rectangular ribs. Air flow with high velocity cannot be mixed completely. Therefore, local heat flux and Nusselt number are lower than the baseline between $x/H=22$ and $x/H=40$. In the delta winglet scenario, the path lines of velocity look different from rectangular rib in Figure 4.9(b), but it is nearly identical before the VGs. The difference of path lines between the rectangular rib scenario and delta winglet scenario can be seen behind the VGs. More vortices are generated after delta winglet VGs, but there are almost less and weaker vortices generated after rectangular rib VGs. From the result that more path lines of velocity are behind delta winglet, it can mix cold and hot air flow more completely in top and bottom boundary layers. The vortices generated after VG interacts with each other for a long distance in the downstream air flow, so cooling performance could be enhanced until air exits the cooling channel.

Figure 4.10 also shows the half-channel cross sections of velocity vector in the rectangular rib scenario and the delta winglet scenario at $x/H=8, 17, 20, 24, 40$ and 80 , respectively. At $x/H=8$ (16mm from inlet), velocity vectors in the delta winglet scenario are very consistent, but velocity is greater in the rectangular ribs at the first cross section. At $x/H=17$, velocity decreases after air crosses the delta winglet VGs, but increases before the delta winglet VGs. The same phenomenon

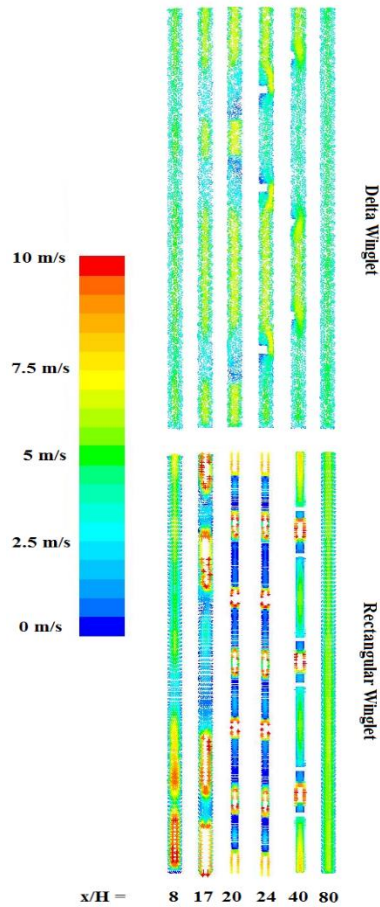


Figure 4. 10 Half-cross sections of velocity vectors

of velocity vectors also presents in the rectangular rib scenario at $x/H=17$, but the velocity is much greater. From $x/H=20$ to $x/H=40$, it can be seen that a counter-rotating pair of vortices are created by the delta winglet VGs on the upper side of each cross section and half-pair of vortices is created on the lower side of each cross section. The right vortices rotate in a counterclockwise direct, while

the left vortices rotate in a clockwise direction. These series of counter-rotating vortices generate the down-wash flow toward the bottom wall of the channel between the vortices and the up-wash flow away from the bottom wall in the region outside of the vortices. Meanwhile, the rotating velocities decrease and the distance between the cores of the vortices increases as the flow moves downstream. The distance between the cores also increases as these vortices move downstream. In the rectangular scenario, it is not obvious that this kind of vortices is generated at the cross section from $x/H=20$ to $x/H=40$. Velocity behind the rectangular VG decreases and increases between each VG, which can cause significant pressure drop after rectangular VGs. It is difficult to mix air flow very well. Therefore, vortices generated by delta winglet VGs cause bulk fluid mixing, boundary-layer modification and flow destabilization, thus improve convective heat transfer.

From the previous results, using vortex generator in the air channel for active cooling of pouch cell, the thermal performance has been evaluated and proved that VG can significantly enhance heat transfer not only in the upstream domain, but also in the downstream domain when delta

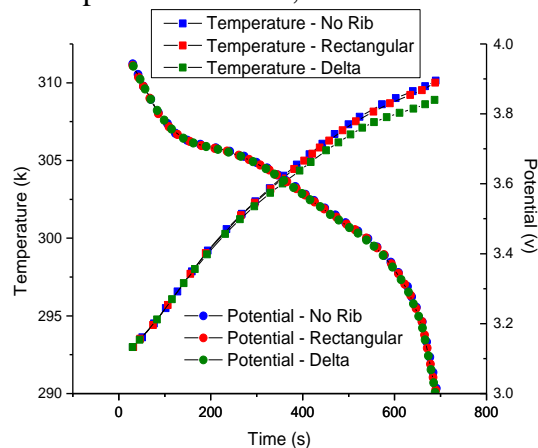


Figure 4. 11 Time-wise maximum cell temperature and potential of pouch cell

winglet is adopted. It is definitely beneficial to the battery, since the control of temperature within a required range is very important to the battery application. Due to the battery mainly used in the electric vehicle and building energy storage, it usually needs the response of battery with high discharging rates. From the numerical study, Figure 4.11 Shows the time-wise temperature and potential comparison between the baseline, rectangular rib and delta winglet scenarios. The time-wise study was just conducted for one discharging cycle, the result shows the different of maximum temperature of pouch cell between the baseline and rectangular ribs after one discharging cycle is nearly 0.5k, but it is 2k between the baseline and delta winglet scenarios. Since the total temperature rise from the beginning of discharge is 293k and changes to 312k after one discharging cycling (700 seconds), the percentage decrease of maximum cell temperature is above 10%. It is due to the enhanced heat transfer by delta winglet deployed on the cell surface. The result from the numerical study also shows that local Nusselt number would be increased by 38% compared to the baseline scenario if delta winglet is used, which is very promising and encouraging to the widely use of delta winglet VG for thermal management in the battery application.

4.6 Conclusion

In this study, numerical simulations have been conducted to explore the air flow and heat transfer in a horizontal rectangular channel with two different configurations of vortex generator at different discharging rates. The simulation results in air flow domain with characteristics of heat transfer and flow structure show that both types of vortex generators can enhance heat transfer before VGs. Detailed results of parametric analysis will be discuss in the Chapter 5.

CHAPTER 5 CONCLUSIONS AND FUTURE STUDIES

5.1 Main results by using fin-like structures in two building energy storages

5.1.1 Main results of thin layer ring application

Although ITS systems have been widely applied in cooling systems to improve energy efficiency and reduce energy cost, the inefficient ice formation still remains a problem in current commercial practices. In this study, novel thin layer ring was proposed to enhance heat transfer during the ice formation process in the ITS system. A numerical study was carried out to investigate the effects of the thin layer ring structure in enhancing the heat transfer during the ice formation process. From the results obtained in this study, the area ratio can be increased by 4% when using the thin layer ring during the same time period, since energy can be transferred from water to the cooled cylinder through the thin layer ring more efficiently. Since heat transfer can be enhanced by many different methods, the novel thin layer ring is used as extended fin to induce energy from not completely cooled region to the cooled cylinder. During the ice formation process, this novel technology has not been analyzed in detail, therefore many different parameters could impact its performance on the solidification of water. Usually, the change in thermal conductivity of material would vary the rate of heat transfer. Meanwhile, the distance of transferring also affects conductive heat transfer within the transferring material. Because of the phase change occurring in an ITS system, it always happens firstly near the cooling source, the strategy or arrangement of transferring material also plays an important role, which needs to be taken into account. This analysis was focused on investigating three different parameters of the thin layer ring structure,

namely the effect of material, thickness and arrangement on the ice formation enhancement. Major findings from this study are summarized as follows:

1. The investigation on the effect of material shows that copper has the best performance among the four tested materials during the same time period of ice formation. Aluminum ranks as the second according to the ice generated area. The third and fourth ones are Magnesium alloy and stainless steel, respectively. From these results, it can be concluded that thermal conductivity of material has significant impact on the performance of the thin layer ring. The ice generated area can be increased by increasing thermal conductivity of materials.
2. The study conducted to analyze the effect of thickness of the thin layer ring shows that 3 mm thin layer ring has the best performance among five selected thickness. The 1 mm case is better than 2 mm case, while both are better than 0.25 mm and 0.5 mm obviously, but not as good as 3 mm thin layer ring. Consequently, the results find that the performance of thin layer ring is dependent on the thickness as well, but there is an optimal thickness for the best heat transfer performance.
3. Analysis of three arrangements shows that the staggered arrangement has the best performance, since it has the longest span-wise distance between the two cooled cylinders. The two parallel arrangements are better than one parallel arrangement, because it has larger heat transfer area than the one parallel arrangement. The performance of the thin layer ring is increased with the increase of heat transfer area.

The impact of the different parameters of thin layer ring on ice formation in a rectangular space has been evaluated and investigated by the numerical method. Moreover, the optimal parameters and condition have been determined by the Taguchi method. The numerical results from this study can be used as a research guideline of the novel structure of thin layer ring applied in ice thermal storage tank for other researchers in their experiments. The main results of Taguchi analysis are concluded below.

The factorial impact of the different parameters of thin layer ring during ice formation using numerical methods has been evaluated. The results show that material has the greatest impact on ice increased area. After that, arrangement has relatively less influence on ice increased area. However, thickness has the trifling effect on ice increased area.

From the study, the optimal combination of each factor (parameter) has been determined, and the optimal condition is A3B2C1. The reproducibility of these conditions has been verified by two analytical results

5.1.2 Main results of vortex generator application

In this study, numerical simulations have been conducted to explore the air flow and heat transfer in a horizontal rectangular channel with two different configurations of vortex generator at different discharging rates. These two configurations of vortex generators are: (1) rectangular rib; (2) delta winglet. The battery model was coupled with three dimensional Navier-Stokes and energy

equations for the analysis of thermal performance and the effect of two types of VG on the cooling enhancement.

The simulation results in air flow domain with characteristics of heat transfer and flow structure show that both types of vortex generators can enhance heat transfer before VGs, but only delta winglet VG can still enhance local heat transfer after it due to more vortices generated that can mix cold and hot air flow between the top and bottom thermal layers completely. These vortices cause bulk fluid mixing, boundary-layer modification and flow destabilization, thus improving convective heat transfer on the surface. The maximum temperature of pouch cell is also numerically investigated by validated battery model. The result shows that the maximum temperature of pouch cell can be decreased more by delta winglet than by rectangular rib. For the discharging rate at 5C, it can be decreased by 10% and the local Nusselt number can be increased by 38% compared to the baseline scenario without any VGs.

5.2 Recommendation for future study

Future work based on the results will take the physical model of thin layer ring into the consideration. The experiments will be carried out to further exam the factorial effect of three parameters, such as thickness, material and arrangement of thin layer ring. In the further study of battery energy storage, other parameters regarding could also be investigated, including cooling flow velocity, VG geometry aspect ratio, attack angle, arrangement of VG, so as to advance the understanding of VG performance and develop design guidelines for the application of vortex-enhanced heat transfer technique in heat exchangers and other energy applications. The cost

analysis of using thin layer ring will be also conducted to evaluate the feasibility of commercialization.

REFERENCES

- "Electric Vehicle Lithium Ion Batteries Thermal Management."
- (1996). Source energy and environmental impacts of thermal energy storage.
- (1998). ACRC TR-137. Air Conditioning and Refrigeration Center, University of Illinois.
- (2007). HVAC Applications, ASHRAE.
- Biswas, G. and H. Chattopadhyay (1992). "Heat transfer in a channel with built-in wing-type vortex generators." International Journal of Heat and Mass Transfer **35**(4): 803-814.
- Biswas, G., N. K. Mitra and M. Fiebig (1989). "Computation of laminar mixed convection flow in a channel with wing type built-in obstacles." Journal of Thermophysics and Heat Transfer **3**(4): 447-453.
- Bortolini, M., M. Gamberi and A. Graziani (2014). "Technical and economic design of photovoltaic and battery energy storage system." Energy Conversion and Management **86**: 81-92.
- Brower, M. (1994). Cool Energy, Massachusetts Institute of Technology Press.
- C.J. Hoogendoorn, G. C. J. B. (1992). "Performance and Modeling of Latent Heat Storage." Solar Energy **48**: 53-58.
- Chaichana, C., W. W. S. Charters and L. Aye (2001). "An ice thermal storage computer model." Applied Thermal Engineering **21**(17): 1769-1778.
- Chang, L.-M., L.-B. Wang, K.-W. Song, D.-L. Sun and J.-F. Fan (2009). "Numerical study of the relationship between heat transfer enhancement and absolute vorticity flux along main flow direction in a channel formed by a flat tube bank fin with vortex generators." International Journal of Heat and Mass Transfer **52**(7-8): 1794-1801.
- Chen, C., J.-T. Teng, C.-H. Cheng, S. Jin, S. Huang, C. Liu, M.-T. Lee, H.-H. Pan and R. Greif (2014). "A study on fluid flow and heat transfer in rectangular microchannels with various longitudinal vortex generators." International Journal of Heat and Mass Transfer **69**: 203-214.
- Chen, F. C., Z. Gao, R. O. Loutfy and M. Hecht (2003). "Analysis of Optimal Heat Transfer in a PEM Fuel Cell Cooling Plate." Fuel Cells **3**(4): 181-188.
- Chiu, J. N.-W., V. Martin and F. Setterwall (2009). "A review of thermal energy storage systems with salt hydrate phase change materials for comfort cooling."

Choi, Y. S. and D. M. Kang (2014). "Prediction of thermal behaviors of an air-cooled lithium-ion battery system for hybrid electric vehicles." Journal of Power Sources **270**: 273-280.

Chu, P., Y. L. He, Y. G. Lei, L. T. Tian and R. Li (2009). "Three-dimensional numerical study on fin-and-oval-tube heat exchanger with longitudinal vortex generators." Applied Thermal Engineering **29**(5): 859-876.

Chu, P., Y. L. He and W. Q. Tao (2009). "Three-Dimensional Numerical Study of Flow and Heat Transfer Enhancement Using Vortex Generators in Fin-and-Tube Heat Exchangers." Journal of Heat Transfer **131**(9): 091903-091903-091909.

Chu, P., Y. L. He and W. Q. Tao (2009). "Three-Dimensional Numerical Study of Flow and Heat Transfer Enhancement Using Vortex Generators in Fin-and-Tube Heat Exchangers." Journal of Heat Transfer **131**(9): 091903-091903.

Davidson, A. S. L. (2001). "EFFECT OF INCLINED VORTEX GENERATORS ON HEAT TRANSFER ENHANCEMENT IN A THREE-DIMENSIONAL CHANNEL." Numerical Heat Transfer, Part A: Applications **39**(5): 433-448.

De-Leon, S. (2010). High power rechargeable lithium battery market.

Divya, K. C. and J. Østergaard (2009). "Battery energy storage technology for power systems—An overview." Electric Power Systems Research **79**(4): 511-520.

E.M. Sparrow, E. D. L., J.W. Ramsey (1984). "Freezing on a finned tube for either conduction-controlled or natural convection controlled heat transfer." International Journal of Heat and Mass Transfer **24**: 273-284.

Egolf, P. W. and M. Kauffeld (2005). "From physical properties of ice slurries to industrial ice slurry applications." International Journal of Refrigeration **28**(1): 4-12.

Fan, L., J. M. Khodadadi and A. A. Pesaran (2013). "A parametric study on thermal management of an air-cooled lithium-ion battery module for plug-in hybrid electric vehicles." Journal of Power Sources **238**(0): 301-312.

Fathabadi, H. (2014). "A novel design including cooling media for Lithium-ion batteries pack used in hybrid and electric vehicles." Journal of Power Sources **245**: 495-500.

Ferrouillat, S., P. Tochon, C. Garnier and H. Peerhossaini (2006). "Intensification of heat-transfer and mixing in multifunctional heat exchangers by artificially generated streamwise vorticity." Applied Thermal Engineering **26**(16): 1820-1829.

- Fiebig, M. (1995). "Embedded vortices in internal flow: heat transfer and pressure loss enhancement." International Journal of Heat and Fluid Flow **16**(5): 376-388.
- Fiebig, M. (1998). "Vortices, Generators and Heat Transfer." Trans IChemE **76**(Part A): 108-123.
- Fiebig, M. (1998). "Vortices, Generators and Heat Transfer." Chemical Engineering Research and Design **76**(2): 108-123.
- Fiebig, M. (1998). "Vortices, Generators and Heat Transfer." Transactions of the American Institute of Chemical Engineers **76**(Part A): 108-123.
- Fiebig, M., U. Brockmeier, N. K. Mitra and T. Gü termann (1989). "STRUCTURE OF VELOCITY AND TEMPERATURE FIELDS IN LAMINAR CHANNEL FLOWS WITH LONGITUDINAL VORTEX GENERATORS." Numerical Heat Transfer, Part A: Applications **15**(3): 281-302.
- Fiebig, M., P. Kallweit, N. Mitra and S. Tiggelbeck (1991). "Heat transfer enhancement and drag by longitudinal vortex generators in channel flow." Experimental Thermal and Fluid Science **4**(1): 103-114.
- Fisher, R. A. (1925). Statistical Methods for Research Worker. London, Oliver & Boyd.
- Gattrell, M., J. Park, B. MacDougall, J. Apte, S. McCarthy and C. W. Wu (2004). "Study of the Mechanism of the Vanadium 4+/5+ Redox Reaction in Acidic Solutions." Journal of The Electrochemical Society **151**(1): A123.
- Giuliano, M. R., A. K. Prasad and S. G. Advani (2012). "Experimental study of an air-cooled thermal management system for high capacity lithium–titanate batteries." Journal of Power Sources **216**: 345-352.
- H-G, B. a. B. S. (2007). "Robust Optimization - A Comprehensive Surve." Computer Methods in Applied Mechanics and Engineering **196**: 34-44.
- H. Akbari, A. M. (1989). Energy Storage System: Fundamentals & Application, Academic Publishers.
- Habeebullah, B. A. (2007). "Economic feasibility of thermal energy storage systems." Energy and Buildings **39**(3): 355-363.
- Hasnain, S. M. (1998). "Review on sustainable thermal energy storage technologies, Part I: heat storage materials and technologies." Energy conversion and management **39**(11): 1127-1138.
- Haughey, M. D. (2003). "Ice Thermal Storage for Colorado School." ASHRAE: 50-53.

Huo, Y., Z. Rao, X. Liu and J. Zhao (2015). "Investigation of power battery thermal management by using mini-channel cold plate." Energy Conversion and Management **89**: 387-395.

Ibrahim, H., A. Ilinca and J. Perron (2008). "Energy storage systems—Characteristics and comparisons." Renewable and Sustainable Energy Reviews **12**(5): 1221-1250.

Ikeda, S. and R. Ooka (2015). "Metaheuristic optimization methods for a comprehensive operating schedule of battery, thermal energy storage, and heat source in a building energy system." Applied Energy **151**: 192-205.

J. Xie, C. Y. (2013). Numerical study of ice formation in ice thermal storage system using thin layer ring. Proceedings of 2013 International Symposium on Green manufacturing and Applications, Honolulu, Hawaii.

Jarrett, A. and I. Y. Kim (2011). "Design optimization of electric vehicle battery cooling plates for thermal performance." Journal of Power Sources **196**(23): 10359-10368.

Joardar, A. and A. M. Jacobi (2005). "Impact of leading edge delta-wing vortex generators on the thermal performance of a flat tube, louvered-fin compact heat exchanger." International Journal of Heat and Mass Transfer **48**(8): 1480-1493.

Joardar, A. and A. M. Jacobi (2006). "A Numerical Study of Flow and Heat Transfer Enhancement Using an Array of Delta-Winglet Vortex Generators in a Fin-and-Tube Heat Exchanger." Journal of Heat Transfer **129**(9): 1156-1167.

Joardar, A. and A. M. Jacobi (2008). "Heat transfer enhancement by winglet-type vortex generator arrays in compact plain-fin-and-tube heat exchangers." International Journal of Refrigeration **31**(1): 87-97.

K.H., H., K.W., Lee (2001). "Robust Optimization of an Automobile Rearview Mirror for Vibration Reduction." Struct. Multidisc. Optim. **21**: 300-308.

Karimi, G. and A. R. Dehghan (2014). "Thermal analysis of high-power lithium-ion battery packs using flow network approach." International Journal of Energy Research **38**(14): 1793-1811.

Karimi, G. and X. Li (2013). "Thermal management of lithium-ion batteries for electric vehicles." International Journal of Energy Research **37**(1): 13-24.

Kintner-Meyer, M., Subbarao, K., Kumar, N.P., Wang, J., Molburg, J.C., Zhao, F., (2010). The Role of Energy Storage in Commercial Building. A Preliminary Report, U.S. Department of Energy.

Lacroix, M. (1993). "Numerical simulation of a shell-and-tube latent heat thermal energy storage unit." Solar Energy **50**(4): 357-367.

Lacroix, M. (1993). "Study of the heat transfer behavior of a latent heat thermal energy storage unit with a finned tube." International Journal of Heat and Mass Transfer **36**(8): 2083-2092.

Lei, Y.-G., Y.-L. He, L.-T. Tian, P. Chu and W.-Q. Tao (2010). "Hydrodynamics and heat transfer characteristics of a novel heat exchanger with delta-winglet vortex generators." Chemical Engineering Science **65**(5): 1551-1562.

Leu, J.-S., Y.-H. Wu and J.-Y. Jang (2004). "Heat transfer and fluid flow analysis in plate-fin and tube heat exchangers with a pair of block shape vortex generators." International Journal of Heat and Mass Transfer **47**(19): 4327-4338.

Liu, C., J.-t. Teng, J.-C. Chu, Y.-I. Chiu, S. Huang, S. Jin, T. Dang, R. Greif and H.-H. Pan (2011). "Experimental investigations on liquid flow and heat transfer in rectangular microchannel with longitudinal vortex generators." International Journal of Heat and Mass Transfer **54**(13-14): 3069-3080.

Lu, L., X. Han, J. Li, J. Hua and M. Ouyang (2013). "A review on the key issues for lithium-ion battery management in electric vehicles." Journal of Power Sources **226**: 272-288.

M.A. Khan, P. K. R. (1994). "Numerical Solution to a Moving Boundary Problem in a Composite Medium." Numerical Heat Transfer **25**: 209-221.

MacCracken, M. M. (2003). "Thermal Energy Storage Myths." ASHRAE Journal **45**(9): 36-43.

Mahamud, R. and C. Park (2011). "Reciprocating air flow for Li-ion battery thermal management to improve temperature uniformity." Journal of Power Sources **196**(13): 5685-5696.

McQuade, J. M. (2009). A system approach to high performance buildings. Tech. Report, United Technologies Corporation.

Mohammadian, S. K. and Y. Zhang (2015). "Thermal management optimization of an air-cooled Li-ion battery module using pin-fin heat sinks for hybrid electric vehicles." Journal of Power Sources **273**: 431-439.

Mori, T. (1990). The New Experimental Design: Taguchi's Approach to Quality Engineering, ASI Press.

Nian, C. Y., W. H. Yang and Y. S. Tarn (1999). "Optimization of turning operations with multiple performance characteristics." Journal of Materials Processing Technology **95**(1-3): 90-96.

- P.V., P. and M. K. M.V. (1986). "Outward phase change in a cylindrical annulus with axial fins on the inner tube." International Journal of Heat and Mass Transfer **29**(12): 1855-1868.
- Park, H. (2013). "A design of air flow configuration for cooling lithium ion battery in hybrid electric vehicles." Journal of Power Sources **239**(0): 30-36.
- Pesaran, G. H. K. a. A. (2006). "Battery thermal management system design modeling."
- Ponce de León, C., A. Frías-Ferrer, J. González-García, D. A. Szánto and F. C. Walsh (2006). "Redox flow cells for energy conversion." Journal of Power Sources **160**(1): 716-732.
- Redindel, D. T. (1996). EPRI International Conference on Sustainable Thermal Energy Storage, Minnesota, USA.
- Reihani, E., S. Sepasi, L. R. Roose and M. Matsuura (2016). "Energy management at the distribution grid using a Battery Energy Storage System (BESS)." International Journal of Electrical Power & Energy Systems **77**: 337-344.
- Rismanchi, B., R. Saidur, H. H. Masjuki and T. M. I. Mahlia (2012). "Thermodynamic evaluation of utilizing different ice thermal energy storage systems for cooling application in office buildings in Malaysia." Energy and Buildings **53**(0): 117-126.
- Ross, P. J. (1988). Taguchi Techniques for Quality Engineering. New York, McGraw-Hill.
- S. Morgan, M. K. (2010). "Field Testing of Optimal Controls of Passive and Active Thermal Storage." ASHRAE **116**: 134-146.
- Saidur, R., H. H. Masjuki and M. Y. Jamaluddin (2007). "An application of energy and exergy analysis in residential sector of Malaysia." Energy Policy **35**(2): 1050-1063.
- Sarah Lichtner, R. B., Lindsay kishter, (2010). Advanced Materials and Devices for Stationary Electrical Energy Storage Applications, U.S. Department of Energy.
- Sasaguchi, K., K. Kusano and R. Viskanta (1997). "A numerical analysis of solid-liquid phase change heat transfer around a single and two horizontal, vertically spaced cylinders in a rectangular cavity." International Journal of Heat and Mass Transfer **40**(6): 1343-1354.
- Seong Kim, U., J. Yi, C. B. Shin, T. Han and S. Park (2011). "Modeling the Dependence of the Discharge Behavior of a Lithium-Ion Battery on the Environmental Temperature." Journal of The Electrochemical Society **158**(5): A611-A618.
- Shears, C. F. (1991). Australian Refrigeration. Air conditioning and heating, Melbourne, Australia, AIRAH.

- Siegel, R. (1977). "Solidification of low conductivity material containing dispersed high conductivity particles." International Journal of Heat and Mass Transfer **20**(10): 1087-1089.
- Smith, J., M. Hinterberger, P. Hable and J. Koehler (2014). "Simulative method for determining the optimal operating conditions for a cooling plate for lithium-ion battery cell modules." Journal of Power Sources **267**(0): 784-792.
- Sommers, A. D. and A. M. Jacobi (2005). "Air-side heat transfer enhancement of a refrigerator evaporator using vortex generation." International Journal of Refrigeration **28**(7): 1006-1017.
- Song, K.-W., L.-B. Wang, J.-F. Fan, Y.-H. Zhang and S. Liu (2008). "Numerical study of heat transfer enhancement of finned flat tube bank fin with vortex generators mounted on both surfaces of the fin." Heat and Mass Transfer **44**(8): 959-967.
- Sumpter, R. S. (1992). Energy Engineering **89**(4).
- Sun, H., X. Wang, B. Tossan and R. Dixon (2012). "Three-dimensional thermal modeling of a lithium-ion battery pack." Journal of Power Sources **206**(0): 349-356.
- T. Collins, S. A. P., D. Brown (2000). Thermal Energy Storage for Space Cooling. Technical Report Produced for the U.S. Department of Energy.
- Taguchi, G. (1989). Quality Engineering in Production Systems. New York, McGraw-Hill.
- Taguchi, G. (1990). Introduction to Quality Engineering. Tokyo, Asian Productivity Organization.
- Taguchi, G. (1991). Taguchi on Robust Technology Development, Bring Quality Engineering (QE) Upstream, ASME.
- Tian, L.-T., Y.-L. He, Y.-G. Lei and W.-Q. Tao (2009). "Numerical study of fluid flow and heat transfer in a flat-plate channel with longitudinal vortex generators by applying field synergy principle analysis." International Communications in Heat and Mass Transfer **36**(2): 111-120.
- Tian, L., Y. He, Y. Tao and W. Tao (2009). "A comparative study on the air-side performance of wavy fin-and-tube heat exchanger with punched delta winglets in staggered and in-line arrangements." International Journal of Thermal Sciences **48**(9): 1765-1776.
- Tiggelbeck, S., N. Mitra and M. Fiebig (1992). "Flow structure and heat transfer in a channel with multiple longitudinal vortex generators." Experimental Thermal and Fluid Science **5**(4): 425-436.

- Tiggelbeck, S., N. K. Mitra and M. Fiebig (1993). "Experimental investigations of heat transfer enhancement and flow losses in a channel with double rows of longitudinal vortex generators." International Journal of Heat and Mass Transfer **36**(9): 2327-2337.
- Torii, K., K. M. Kwak and K. Nishino (2002). "Heat transfer enhancement accompanying pressure-loss reduction with winglet-type vortex generators for fin-tube heat exchangers." International Journal of Heat and Mass Transfer **45**(18): 3795-3801.
- Wang, L., Z. Wang and R. Yang (2012). "Intelligent Multiagent Control System for Energy and Comfort Management in Smart and Sustainable Buildings." IEEE Transactions on Smart Grid **3**(2): 605-617.
- Wang, Q., Q. Chen, L. Wang, M. Zeng, Y. Huang and Z. Xiao (2007). "Experimental study of heat transfer enhancement in narrow rectangular channel with longitudinal vortex generators." Nuclear Engineering and Design **237**(7): 686-693.
- Webb, R. L. (1994). Principles of Enhanced Heat Transfer. New York, John Wiley and Sons.
- Wu, J. M. and W. Q. Tao (2007). "Investigation on laminar convection heat transfer in fin-and-tube heat exchanger in aligned arrangement with longitudinal vortex generator from the viewpoint of field synergy principle." Applied Thermal Engineering **27**(14): 2609-2617.
- Wu, J. M. and W. Q. Tao (2007). "Investigation on laminar convection heat transfer in fin-and-tube heat exchanger in aligned arrangement with longitudinal vortex generator from the viewpoint of field synergy principle." Applied Thermal Engineering **27**(14–15): 2609-2617.
- Xie, J. and C. Yuan (2014). "Numerical study of thin layer ring on improving the ice formation of building thermal storage system." Applied Thermal Engineering **69**(1–2): 46-54.
- Xu, X. M. and R. He (2013). "Research on the heat dissipation performance of battery pack based on forced air cooling." Journal of Power Sources **240**: 33-41.
- Xun, J., R. Liu and K. Jiao (2013). "Numerical and analytical modeling of lithium ion battery thermal behaviors with different cooling designs." Journal of Power Sources **233**: 47-61.
- Yamaha, M., N. Nakahara and R. Chiba (2008). "Studies on thermal characteristics of ice thermal storage tank and a methodology for estimation of tank efficiency." International Journal of Energy Research **32**(3): 226-241.
- Yang, H., H. Bang, K. Amine and J. Prakash (2005). "Investigations of the Exothermic Reactions of Natural Graphite Anode for Li-Ion Batteries during Thermal Runaway." Journal of The Electrochemical Society **152**(1): A73-A79.

Zhu, J. X., M. Fiebig and N. K. Mitra (1993). "Comparison of Numerical and Experimental Results for a Turbulent Flow Field With a Longitudinal Vortex Pair." Journal of Fluids Engineering **115**(2): 270-274.

Zhu, J. X., N. K. Mitra and M. Fiebig (1993). "Effects of longitudinal vortex generators on heat transfer and flow loss in turbulent channel flows." International Journal of Heat and Mass Transfer **36**(9): 2339-2347.

CURRICULUM VITAE

Julian Junling Xie

EDUCATION

- Ph.D. Mechanical Engineering
 - University of Wisconsin Milwaukee (UWM) 08/2017
 - Ph.D. Thesis: Numerical Study of Thermal Storage and Distributed Energy Storage Systems with PV and EV Integration for Demand Response
- M.S. Mechanical Engineering
 - Lawrence Technological University, Michigan 06/2012
 - M.S. Thesis: A Numerical Study of Air-Side Heat Transfer Enhancement using V-Formation Delta-Winglet Vortex Generators in Heat Exchanger
- B.S. Mechanical Engineering (Automotive Engineering)
 - Shanghai University of Engineering Science 06/2009
- B.A. English Language & Literature
 - Shanghai International Studies University 06/2009

RESEARCH EXPERIENCE

Laboratory for Sustainable and Nano-Manufacturing, UWM May 2012 – August 2017

- Ph.D. Thesis: Heat Transfer Optimization in Building Energy Storage Systems
 - Analyzed energy use before & after installation of two energy storage systems (thermal storage and battery storage)
 - Evaluated operational costs of building energy storage projects
 - Tested different materials to improve building energy efficiency using energy storage systems
 - Designed a new mechanical structure in building thermal storage system for the performance improvement
 - Created a model of building thermal storage system with CATIA and ANSYS
 - Quantified heat transfer enhancement and ice formation rate numerically in building thermal storage system
 - Designed a new mechanical structure in battery energy storage system for the cooling enhancement
 - Quantified heat transfer rate and pressure drop penalty in battery energy storage system
- Mechanical Systems Research: Energy Efficiency Studies on Various Mechanical Systems
 - Conducted existing mechanical systems analysis by using different data loggers for data collection
 - Interpreted data (amps, voltage, temperature, etc.) using professional software for existing power consumption
 - Created energy models for various mechanical systems using collected data
 - Optimized energy efficiency of various mechanical systems by modifying or replacing existing systems
 - Verified energy efficiency improvement by measuring data with different data sensors

- Renewable Energy Technologies Research: Integration of microgrid system with renewable energy technologies
 - Investigated electricity demand management with thermal energy storage and distributed energy storage
 - Analyzed microgrid systems with integration of distributed energy, solar PV technology and electric vehicle

Thermal and Fluid Laboratory, Lawrence Technological University Sept. 2010 – June 2012

- M.S. Thesis: A Numerical Study of Air-Side Heat Transfer Enhancement using V-Formation Delta-Winglet Vortex Generators in Heat Exchanger
 - Designed V-Formation Delta-Winglet Vortex Generators
 - Completed detailed drawings with CATIA and SOLIDWORKS
 - Analyzed heat transfer enhancement and pressure drop penalty in a channel flow with ANSYS FLUENT
 - Performed numerical simulation to validate the experimental accuracy in the channel of heat exchanger

PROFESSIONAL, LEADERSHIP EXPERIENCE

Franklin Energy Services, LLC – Mequon, Wisconsin

May 2016 – June 2017

- Energy Engineer Intern:
 - Developed and maintained databases for the New York rebate programs and Michigan Energy Database
 - Reviewed and edited the report template of Energy Plan for the new rebate programs for Illinois programs
 - Created operation documents for the new rebate programs, such as calculator, operation checklist, and internal operation manual
 - Created energy models to provide technical assistance for design, retrofit and replacement of different systems
 - Cooperated with trade allies to design, evaluate and implement energy efficient systems (building insulation, lighting, boiler, air make-up unit, HVAC, thermal oxidizer, oven, furnace), and provided the technical review of contractors and customers' submitted documents for the rebate approvals

U.S. DOE, Industrial Assessment Center – UWM

May 2012 – August 2017

- Lead Energy Engineer:
 - Supervised, coordinated, and managed day-to-day operations of a team of 15 engineers
 - Performed over 50 on-site industrial energy assessments in order to find possible opportunities for energy savings, productivity increase and waste minimization
 - Conducted detailed data analysis on industrial energy systems, including building insulation, compressed air, cooling system, heating system, HVAC, boiler, furnace, lighting, etc.
 - Utilized Onset HOB0 data loggers and sensors at each plant to measure power consumption, current, temperature, and humidity, as well as other advanced metering equipment such as combustion analyzer, ultrasonic compressed air leak detector, infrared gun, thermal image camera, and air flow meter
 - Analyzed collected data, utility bills for the time of use, electricity consumption, natural gas consumption and water consumption to determine possible energy conservation measures
 - Investigated federal, state, and utility incentive programs and rebates for the project implementation

- Communicated and collaborated with clients' senior management, utility providers, and equipment vendors for technical and feasibility analysis, economic analysis, energy incentives and utility rebates
- Supervised the assessment report writing including current energy consumption, proposed energy consumption, cost savings, implementation cost, and associated payback periods
- Interviewed and trained new team members and plant personnel focused on identifying and resolving energy and process related issues, as well as improving and sustaining safety procedures
- Assisted with renewal proposal writing successfully procuring \$2,000,000 of U.S DOE funding
- Testimony: <http://uwm.edu/news/companies-team-up-with-uwm-to-consume-energy-cut-costs/>

Society of Automotive Engineers, Lawrence Technological University Feb. 2010 – June 2011

- Formula SAE Project: Fuel System Design, drawing and installation

Shanghai Automotive Engineering Training Center, SUES May 2007 – June 2009

- Honda Econo Power Project:
 - Designed, drew, and manufactured a three-wheel vehicle
 - Challenged the fuel efficiency of designed vehicle (493 MPG)
- 1.4L Engine Project: Designed and drew a 1.4L vehicle engine (Design team leader)

ORGANIZATIONS & CERTIFICATION PROGRAMS

Organizations:

- The American Society of Mechanical Engineers (ASME)
- The American Society of Heating Refrigerating and Air-Conditioning Engineers (ASHRAE)
- The Association of Energy Engineers (AEE)
- U.S. Green Building Council
- World Energy Engineers Conference Scholar (WEEC), Orlando, FL, 2015

Certification programs:

- Advanced Steam System Analysis and Qualified Specialist Training, U.S. DOE
- Participation of Industrial Assessment Center, U.S. DOE

HONORS & AWARDS

ASME Student Travel Award

- The American Society of Mechanical Engineers, MSEC, June, 2015

Annual Research Colloquium Travel Award

- The University of Dayton, April, 2016

UWM Graduate Student Travel Grant

- University of Wisconsin, June 2013, June 2015

Annual Student Research Poster Competition (Honorable Mentions)

- College of Engineering & Applied Science, University of Wisconsin, 2014, 2015

UWM Chancellor's Graduate Student Award

- University of Wisconsin, 2013, 2014, 2015

1st, 2nd, and 3rd class of Scholarship (TOP 3%)

- Shanghai University of Engineering Science 2005, 2006, 2007, 2008, 2009

Shanghai Outstanding Graduate Award

PUBLICATIONS

1. Xie, J.L. Liu, L.P. "A Numerical Study of Air-Side Heat Transfer Enhancement using V-Formation Delta-Winglet Vortex Generators in Heat Exchangers", *Proceedings of the ASME 2011 International Mechanical Engineering Congress & Exposition*, Denver, Colorado, US, Paper No. IMECE2011-65862, 2011.
2. Xie, J.L. Yuan, C. "Numerical Study of Ice Formation in Ice Thermal Storage System using Thin Layer Ring", *Proceedings of 2013 International Symposium on Green Manufacturing and Applications*, Honolulu, Hawaii, U.S., July 25-29, 2013.
3. Xie, J.L. Yuan, C. "Study of Thin Layer Ring Materials on Improving the Ice Formation of Thermal Storage System", *Proceedings of 2013 International Conference on Materials, Architecture and Engineering Technology*, Beijing, China, December 19-20, 2013.
4. Xie, J.L. Yuan, C. "Factorial Study of Thin Layer Ring on Improving Thermal Performance of Building Thermal Storage System", *Proceedings of 2015 International Manufacturing Research Conference*, Charlotte, NC, US, June 8-12, 2015.
5. Xie, J.L. Yuan, C. "Numerical study of thin layer ring on improving the ice formation of building thermal storage system", *Applied Thermal Engineering*, 69, 46-54, 2014.
6. Xie, J.L. Yuan, C. "Parametric Study of Ice Thermal Storage System with Thin Layer Ring by Taguchi Method", *Applied Thermal Engineering*, 98, 246-255, 2016.
7. Xie, J.L. Yuan, C. "Numerical Study of Heat Transfer Enhancement using Vortex Generator for Thermal Management of LIB Battery", (Ready for Publication).